Solution conditions determine the relative importance of nucleation and growth processes in α-synuclein aggregation

Alexander K. Buell[a], Céline Galvagnion[a], Ricardo Gaspar[b], Emma Sparr[b], Michele Vendruscolo[a], Tuomas P. J. Knowles[a], Sara Linse[c], and Christopher M. Dobson[a,1]

[a]Department of Chemistry, University of Cambridge, Cambridge CB2 1EW, United Kingdom; and Departments of [b]Physical Chemistry and [c]Biochemistry and Structural Biology, Lund University, SE221 00 Lund, Sweden

Edited by Jonathan S. Weissman, University of California, San Francisco, Howard Hughes Medical Institute, and California Institute for Quantitative Biosciences, San Francisco, CA, and approved March 27, 2014 (received for review August 13, 2013)

The formation of amyloid fibrils by the intrinsically disordered protein α-synuclein is a hallmark of Parkinson disease. To characterize the microscopic steps in the mechanism of aggregation of this protein we have used in vitro aggregation assays in the presence of preformed seed fibrils to determine the molecular rate constant of fibril elongation under a range of different conditions. We show that α-synuclein amyloid fibrils grow by monomer and not oligomer addition and are subject to higher-order assembly processes that decrease their capacity to grow. We also find that at neutral pH under quiescent conditions homogeneous primary nucleation and secondary processes, such as fragmentation and surface-assisted nucleation, which can lead to proliferation of the total number of aggregates, are undetectable. At pH values below 6, however, the rate of secondary nucleation increases dramatically, leading to a completely different balance between the nucleation and growth of aggregates. Thus, at mildly acidic pH values, such as those, for example, that are present in some intracellular locations, including endosomes and lysosomes, multiplication of aggregates is much faster than at normal physiological pH values, largely as a consequence of much more rapid secondary nucleation. These findings provide new insights into possible mechanisms of α-synuclein aggregation and aggregate spreading in the context of Parkinson disease.

seeding | prion-like behavior | neurodegenerative disease | kinetic analysis | electrostatic interactions

The conversion of soluble peptide and protein molecules into insoluble amyloid fibrils is of great interest in fields of science ranging from molecular medicine to nanotechnology (1). The formation of amyloid fibrils is a characteristic feature of a substantial number of increasingly common medical disorders, including neurodegenerative conditions such as Alzheimer's and Parkinson diseases (2). Elucidating the fundamental mechanistic steps involved in the conversion from the soluble to the fibrillar forms of the peptides and proteins involved in such disorders is crucial for understanding their origin and proliferation, and hence for exploring in a rational manner new and effective therapeutic strategies through which to combat their onset or progression (3).

One general aspect of amyloid diseases is that once the first aggregates are formed it is very difficult to stop or reverse the aggregation process. This implies that aggregation needs to be studied in both the absence and presence of preformed aggregates, commonly known as seeds, to deepen our understanding of the mechanism of the self-assembly process in vivo. It is possible to define from in vitro studies the rate constants for the multiplicity of microscopic steps that increase the number and total mass of the different types of aggregates that are populated during this process. Such an analysis has recently been carried out for the Aβ42 peptide (4) associated with Alzheimer's disease by combining experimental and theoretical methodologies. A major finding of that study is that the production of toxic oligomeric species, which can also subsequently convert into fibrillar aggregates, does not result solely from primary nucleation, but is catalyzed by the presence of mature amyloid fibrils, a process known as secondary nucleation (5–8). This auto-catalytic mechanism dominates the aggregation process of Aβ42 under quiescent solution conditions (4). These results show that the overall kinetics of aggregation of Aβ42 are determined by a complex combination of primary and secondary processes, as well as by the growth of oligomeric nuclei and fibrils.

It would be highly desirable to achieve for α-synuclein a level of understanding similar to that now obtained for Aβ42. It has been found, however, that it is extremely challenging to obtain reproducible kinetic data for α-synuclein aggregation in vitro (9–11), except at mildly acidic pH values and in the presence of hydrophobic surfaces (12). In the present article, we investigate the aggregation of α-synuclein in the presence of preformed seeds. Our approach is based on the systematic variation in the quantities of seed fibrils, the monomer concentration, and the solution conditions. We find for α-synuclein at neutral pH and in the absence of other factors, such as agitation or surfactants, that the growth of existing aggregates and higher-order assembly of fibrils occur at much greater rates than either primary nucleation or secondary processes. However, at mildly acidic pH values secondary nucleation is strongly accelerated, changing the overall mechanistic character of the aggregation process.

Significance

The deposition of α-synuclein as insoluble amyloid fibrils and the spreading of such species in the brain are two hallmarks of Parkinson disease. It is therefore of great importance to understand in detail the process of aggregation of this protein. We show by a series of in vitro measurements that amyloid fibrils of α-synuclein can grow under a wide range of solution conditions but that they can multiply rapidly only under a much more select set of solution conditions, mimicking those in endosomes and other organelles. The quantitative characterization of α-synuclein aggregation described here provides new insights into the microscopic mechanisms underlying α-synuclein aggregation in the context of Parkinson disease.

Author contributions: A.K.B., E.S., M.V., T.P.J.K., S.L., and C.M.D. designed research; A.K.B., C.G., and R.G. performed research; A.K.B. and C.G. contributed new reagents/analytic tools; A.K.B., E.S., M.V., T.P.J.K., S.L., and C.M.D. analyzed data; and A.K.B., C.G., R.G., E.S., M.V., T.P.J.K., S.L., and C.M.D. wrote the paper.

The authors declare no conflict of interest.

This article is a PNAS Direct Submission.

Freely available online through the PNAS open access option.

[1]To whom correspondence should be addressed. E-mail: cmd44@cam.ac.uk.

This article contains supporting information online at www.pnas.org/lookup/suppl/doi:10.1073/pnas.1315346111/-/DCSupplemental.

Results

Seeded Experiments Simplify the Kinetic Analysis. It has been widely established that the rate of conversion of soluble proteins into amyloid fibrils can often be strongly accelerated by the addition of preformed seed fibrils (13, 14); this type of phenomenon is also well known in related processes, notably crystallization (15). The addition of seeds may accelerate the aggregation process by at least two different mechanisms: elongation and surface-catalyzed secondary nucleation. The presence of seeds eliminates the need for primary nucleation, and the length of the lag phase decreases with increasing seed concentration. In the presence of a large number of seeds (compared with the number of species formed by primary nucleation or secondary processes during the time course of the experiment), the aggregation profile is expected to be a single exponential function (14) (*SI Appendix*, section 2). This behavior is a consequence of the fact that the number of growth-competent fibril ends remains constant throughout the duration of the experiment; the rate of fibril elongation then varies solely with the concentration of soluble protein, which is progressively depleted during the reaction. Primary nucleation is often much slower than elongation, as a consequence of the higher energy barriers for de novo formation of clusters and aggregates compared with the addition onto an existing template (16, 17), and plays no significant role in the strongly seeded regime. If the length distribution, and hence the number of growing ends of the seed fibrils, is defined it is possible to determine the absolute molecular rate constants of fibril elongation.

It has been shown previously that amyloid fibril fragmentation for many proteins can be strongly enhanced by mechanical action, such as shaking or sonication of the solution, and that after prolonged exposure to such mechanical stresses the length distribution tends toward a limit that is solely determined by the mechanical properties of the fibrils (18). We make use of this feature in the present study to manipulate the average length of the fibrils to obtain a narrow distribution of short seed fibrils (Fig. 1 and *SI Appendix*, section 9). The exceptional reproducibility of aggregation time courses between independent batches of seed fibrils that can be achieved with such an approach is demonstrated in *SI Appendix*, section 5. The high degree of reproducibility of these experiments allows the effects of changes in internal and external conditions to be measured with great accuracy.

α-Synuclein Fibril Elongation Occurs by Monomer Addition. We first investigated the dependence of the elongation rate on the concentration of soluble protein molecules and observed a linear relationship at low concentrations and saturation at higher concentrations (Fig. 2 *A* and *B*). This overall sublinear behavior is similar to that observed for other proteins, including the Sup35 yeast prion (20), S6 (21), insulin, and α-lactalbumin (22). The saturation of the elongation rate with monomer concentration, reminiscent of two-step Michaelis–Menten behavior observed in enzyme kinetics, has been shown to stem from the diffusive nature of the elongation reaction; the incorporation of a monomer onto the end of a growing fibril can be described as the crossing of a single free energy barrier associated with an intrinsic timescale that is of the order of hundreds of microseconds (22), the inverse of which is the prefactor of the limiting elongation rate (22). If the data obtained in the present study for α-synuclein are fitted to this model, which is described by the equation $r(m) = r_{max} m/(m_{1/2} + m)$, we obtain a value of 46 μM for $m_{1/2}$, the concentration at half maximal rate, r_{max}. In *SI Appendix*, section 6 we discuss how this quantity displays a dependence on the conditions of the experiment.

It has been proposed that amyloid fibrils of different proteins, including α-synuclein (23, 24), can grow most efficiently by the addition of oligomers to the fibril ends. In our experiments we used α-synuclein isolated by gel filtration whose CD spectrum is completely consistent with an unfolded monomeric protein (*SI Appendix*, section 3). Therefore, the kinetic analysis in this work as well as similar analyses in earlier studies (20–22) suggests that, at least under the conditions of these experiments, amyloid fibrils of α-synuclein grow primarily by such addition. The molecular rate constant of fibril elongation by monomer addition, k_+, could be determined from the ThT fluorescence time courses of seeded aggregation, together with an analysis of the seed fibril length distribution, and is $\sim 2 \times 10^3$ $M^{-1} \cdot s^{-1}$, corresponding to an average length increase of ∼1 nm/min (at 20 μM; *SI Appendix*, section 8).

α-Synuclein Aggregation at Neutral pH Is Dominated by Fibril Elongation. Having established the highly quantitative and reproducible nature of seeded aggregation of α-synuclein, we designed further experiments in PBS buffer at neutral pH to obtain insights into the relative significance of the other molecular processes that are generally important in filamentous growth, in particular primary nucleation and secondary processes such as fibril fragmentation (7, 25) and monomer-dependent secondary nucleation (4, 6). We systematically decreased the concentration of seed fibrils, and therefore the rate of consumption of monomer by fibril elongation, under quiescent conditions (Fig. 2*C*). The experiments without added seed fibrils show no detectable increase in ThT fluorescence over the timescale used here (up to 40 h), consistent with data from earlier studies under quiescent conditions (9). Moreover, a global fit of the dataset to a model that considers only the elongation of seed fibrils and has a single free parameter, the elongation rate constant, reproduces very well the overall scaling behavior, as shown in Fig. 2*C*. In addition, the early time behavior ($t \leq 1$ h) is in excellent agreement with elongation being the dominant process, as illustrated by the linear scaling of the initial aggregation rate with the concentration of seed fibrils (Fig. 2*C*). It is evident, however, that elongation alone is not able to explain every detail of the complete dataset shown in Fig. 2*C*.

During the experiments involving seeded aggregation, macroscopic gel-like assemblies of fibrils were observed, notably at high protein and high salt concentrations. The fluorescence experiments were performed with an optical fiber positioned below the sample (bottom optics; *Materials and Methods*) and flocculation of fibrils, followed by aggregation and sedimentation of the flocs, would be expected to enhance the fluorescence signal relative to a spatially homogeneous sample. In addition, the formation of an amyloid gel is likely to affect both the mobility of the soluble protein molecules and the accessibility of the fibril ends, and therefore to decrease the overall rate of conversion from soluble to aggregated protein; these phenomena are likely to be the origin of the deviation from simple exponential behavior observed in the data in Fig. 2.

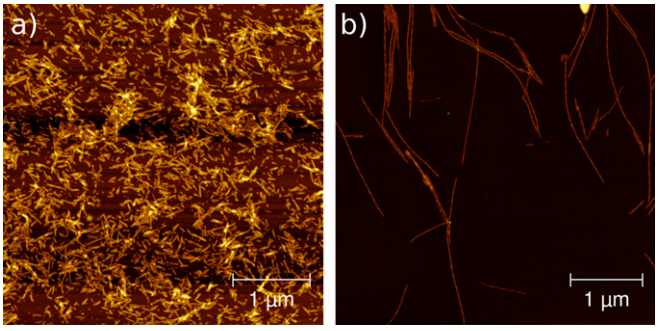

Fig. 1. Atomic force microscopy images, acquired with tapping mode in air, of (*A*) typical mature seed fibrils (formed at pH 6.5) and (*B*) of a low concentration of seed fibrils after prolonged exposure to monomeric α-synuclein, deposited onto mica; see *Materials and Methods* for details on the preparation of the seed fibrils and *SI Appendix*, section 4 for a discussion of the influence of the solution conditions on the properties of the seeds. The fibrils (*A* and *B*) have an average height of ∼7 nm and exhibit the typical dimensions and twist of mature α-synuclein amyloid fibrils that consist of several protofilaments (19).

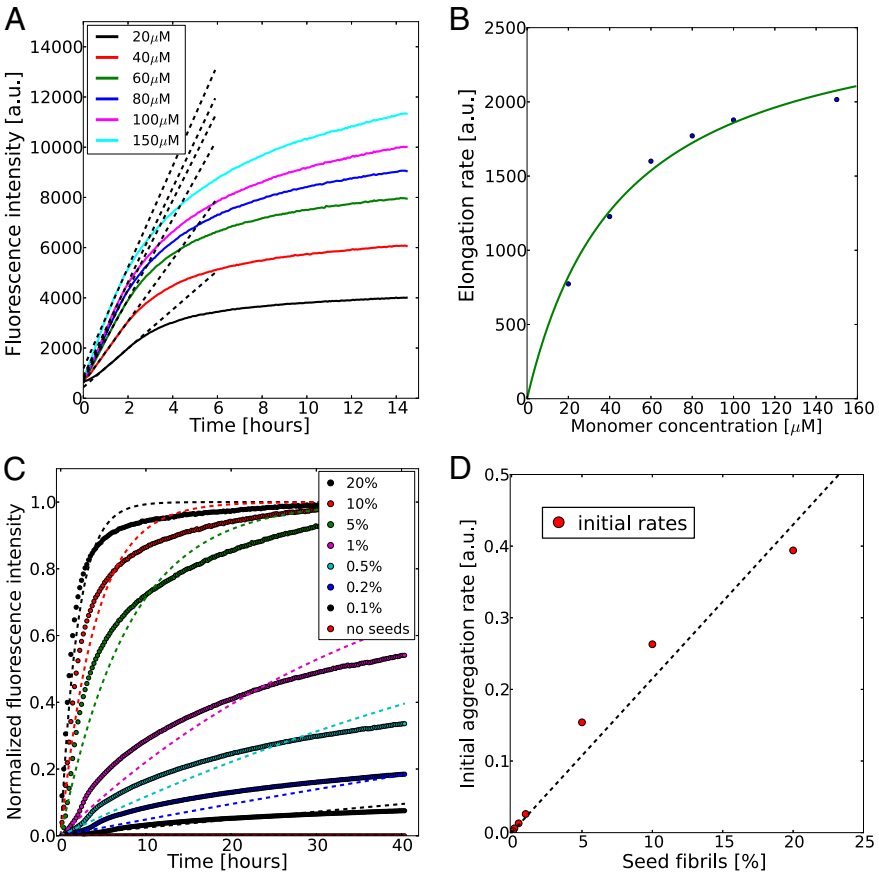

Fig. 2. α-Synuclein fibril elongation occurs by monomer addition and is the dominant growth process at neutral pH. (*A*) Variation of the concentration of soluble (monomeric) protein at constant seed concentration (30 °C, 3.5 μM seed fibrils, PBS buffer, quiescent conditions). (*B*) The elongation rate as a function of the concentration of soluble protein is initially linear and then starts to saturate. The rates have been extracted through linear fits to the early times of the dataset and the concentration at which the elongation rate has reached half of its maximal value was determined to be 46 μM under these conditions. (*C*) Variation of seed concentration at constant monomer concentration (50 μM monomer, 37 °C, PBS buffer, quiescent conditions). The seed concentrations are expressed as percentages of the concentration of soluble protein. A global fit is shown that takes into account only elongation (dotted lines); the model reproduces well the overall scaling of the dataset but does not describe all of its features, therefore indicating that other processes, in particular the higher-order assembly of fibrils, are at play (discussed in the text). (*D*) The initial aggregation rates as a function of the concentration of seed fibrils.

We investigated these processes further by repeating the experiments shown in Fig. 2 in 20 mM phosphate buffer (PB) without added NaCl (*SI Appendix*, Fig. S9*A*), where no macroscopic assemblies of fibrils were visible even at the end of the experimental measurements. In *SI Appendix*, Fig. S9 *C* and *D* we show a comparison of spatially resolved absorbance measurements of aggregated samples in PB and PBS that clearly illustrates a homogeneous distribution of fibrils in the former and an inhomogeneous distribution in the latter case, suggesting that the higher-order assembly of fibrils is less pronounced in the absence of added salt; indeed, the dataset acquired without added NaCl is better described by an elongation-only model than that shown in Fig. 2*C*. To determine the timescale over which the higher-order assembly of fibrils and subsequent enhanced sedimentation can occur, we performed a seeded aggregation experiment with top and bottom optics simultaneously (*SI Appendix*, Fig. S9*B*). In the absence of NaCl, the bottom and top readings yield superimposable curves over timescales of several hours, whereas for PBS the data start to deviate just minutes after the start of the experiments, indicating sample inhomogeneities of the order of hundreds of micrometers. To illustrate this process even more clearly, we monitored seeded aggregation experiments under different conditions in microcapillaries, using an inverted fluorescence microscope, and found that in the confined space of a capillary the flocculation of α-synuclein fibrils into microscopic aggregates is followed by gelation that results from irreversible interaction of the fibril flocs; videos of these experiments can be found in Movies S1–S6.

The conclusion from these experiments is that α-synuclein fibrils can behave under some solution conditions as unstable colloidal suspensions, and so tend to aggregate into larger structures that can subsequently form gels. This process is readily observed under conditions of physiological salt concentrations where the electrostatic repulsion between the fibrils, which are likely to have a similar charge density to the monomer, is strongly screened.

Primary Nucleation and Fragmentation Can Be Selectively Enhanced. Previous work has shown that the process of nucleation of α-synuclein amyloid fibrils is likely to be heterogeneous and catalyzed by environmental features, such as air–water interfaces (26, 27), lipid bilayers (28), SDS micelles and other anionic surfactants (11, 29, 30), or artificial interfaces such as the coatings of containers or stir bars (31). In addition, mechanical action, such as shaking and stirring, is often used to accelerate the aggregation of α-synuclein (32). For the latter type of conditions, it is likely that the mechanical action influences primary nucleation (33) (e.g., through a disturbance of the air–water interface) and also secondary processes [e.g., through an enhanced rate of fragmentation (4)]. To investigate these phenomena, we conducted a series of seeded experiments in the presence of beads of 1–2 mm in size (with periodic shaking cycles; *Materials and Methods*).

To test whether or not the effect on aggregation of the addition of beads stems from the additional surface area introduced into the system, we used beads made from two different materials, hydrophobic Teflon and hydrophilic glass (Fig. 3 *A* and *B*). To distinguish the effects of the beads on primary nucleation and on fragmentation, we performed control experiments without seed fibrils, as well as carrying out the equivalent experiments without added beads. In the absence of any added beads, we observe behavior analogous to that shown in Fig. 2, namely, no detectable increase in fluorescence without added seeds, and approximately linear behavior for low seed concentrations (0.1% by mass), indicating that the shaking protocol used here is not sufficient to induce aggregation under these conditions. However, in the presence of beads, aggregation is observed even without addition of seed fibrils. Furthermore, the plots from experiments carried out in the presence of 0.1% seed fibrils show pronounced

convex behavior, characteristic of an increase with time in the number of growing aggregates. The observation that the seeded aggregation experiments show an acceleration in the fluorescence signal several hours before the unseeded reactions show any significant fluorescence strongly suggests that the dominant effect of the addition of beads is to increase the fibril fragmentation rate (4). Based on these data, it is not, however, possible to exclude some effect of the beads on the process of primary nucleation. Nevertheless, any such effect is likely to be indirect, for example through a disturbance of the air–water interface, rather than the result of a direct surface-catalysis process on the beads, given that the surface hydrophobicity of the beads has little influence on their effects on the aggregation process.

We also performed seeded and unseeded aggregation experiments in the presence of 1 mM SDS under quiescent conditions (Fig. 3*D*), obtaining exponential and sigmoidal aggregation curves, respectively. These results suggest that the presence of SDS strongly enhances the primary nucleation of α-synuclein amyloid fibrils, potentially through the opening of an alternative nucleation pathway, possibly coaggregation with SDS, whereas both the pathway and the free energy barrier for seed fibril elongation remain unaffected. These findings are in line with earlier studies (11, 30, 34) and show that both primary and secondary processes in aggregating α-synuclein at neutral pH can be strongly influenced by a variety of factors and solution conditions.

Rates of Secondary Nucleation Processes in α-Synuclein Aggregation Show a Dramatic pH Dependence. We next investigated the kinetics of seeded aggregation in PBS buffer in a regime of very low seed concentrations (Fig. 4*A*). We decreased the concentration of seed fibrils to a situation where, in the absence of primary nucleation and secondary processes, each seed fibril would in theory have to grow to a final length of 10^3 to 10^4 times its initial length to convert all of the available soluble protein molecules into fibril mass (i.e., nanomolar seed concentration vs. micromolar monomer concentration). In these experiments, we varied the concentrations of both soluble protein and of fibrils. Fig. 4*A* shows a global fit to a kinetic model where the elongation rate varies linearly with the concentration of seed fibrils (as in Fig. 2*D*) and sublinearly with the concentration of soluble monomer (as in Fig. 2*B*), using the saturation concentration of elongation, $m_{1/2}$, and the elongation rate constant k_+ as fitting parameters. This model gives a better global fit than in the case of the higher seed concentrations and the value of $m_{1/2}$ determined here is in remarkable agreement with that determined from the experimental data shown in Fig. 2*B* (49.8 μM vs. 45.8 μM), given the well-known difficulties of determining such asymptotic quantities from hyperbolic relationships (35). At these low seed concentrations, the depletion of monomer by elongation of the fibrils is slow compared with the higher-order assembly of fibrils that can interfere with elongation. Interestingly, the global fit in Fig. 4 yields a lower elongation rate constant k_+ ($\sim 4 \times 10^2$ $M^{-1} \cdot s^{-1}$) compared with that from the fit in Fig. 2*C* (2.2×10^3 $M^{-1} \cdot s^{-1}$; see *SI Appendix*, sections 8 and 11 for details on the fits), even though the experiments have been carried out under very similar solution conditions. Indeed, a detailed look at the data reveals that the rates of increase in fluorescence are slightly higher at the beginning, compared with at the end, of the experiment, leading to a small deviation between the fit and the data at the earlier times. These results are in agreement with the hypothesis put forward above that the higher-order assembly effectively decreases the overall seeding efficiency over time.

We then performed seeded aggregation experiments in PB at low ionic strength (10 mM) as a function of pH, ranging from 4.8 to 6.2, at low seed concentrations (0.04% by mass, Fig. 4*B*). We observed that some of the kinetic traces, in the pH range 4.8–5.6, show clear signs of positive curvature, a finding that suggests that secondary processes are much more pronounced at mildly acidic compared with neutral pH. To investigate this phenomenon further, we carried out kinetic experiments with systematic variations in the concentrations of both soluble and fibrillar protein, similar to those shown in Fig. 4*A*, at pH 5.2, where the positive curvature observed in Fig. 4*B* is maximal. We see very strong positive curvature throughout the entire dataset, confirming the contribution of a secondary process to the aggregation mechanism.

Because of the current lack of a mathematical model of secondary nucleation processes of the type described here, the

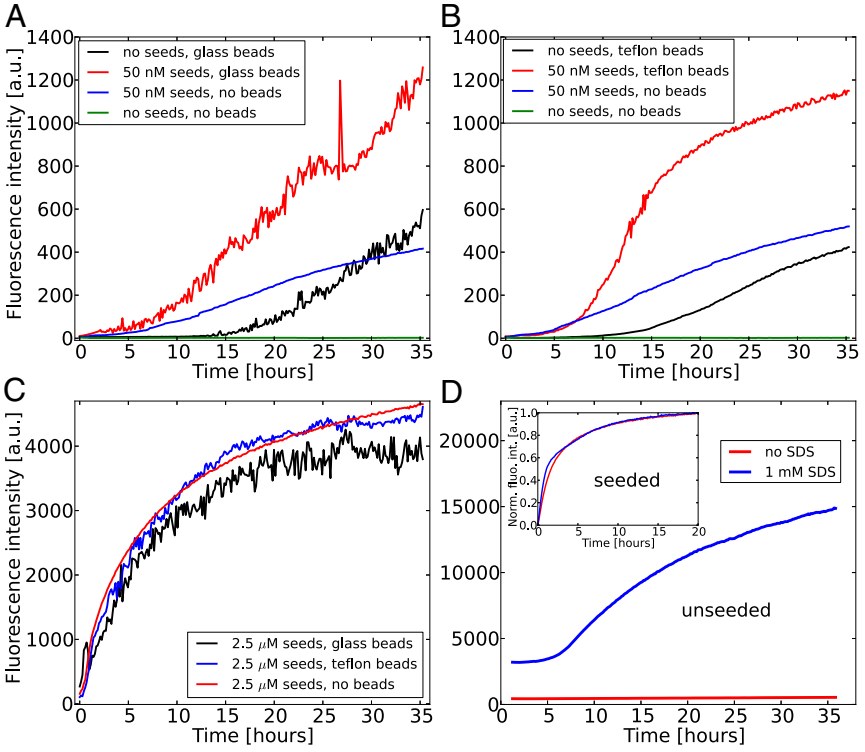

Fig. 3. Primary nucleation and fragmentation in α-synuclein aggregation can be selectively enhanced. Seeded aggregation (50 μM monomer, 50 nM seeds, 37 °C, PBS, shaking) in the presence of beads made from glass (*A*) and Teflon (*B*) in the wells of the plates. (*C*) At higher seed concentrations (5% by mass), the presence of the beads has little effect on the kinetics. (*D*) 1 mM SDS induces aggregation under quiescent conditions (PB, 75 μM α-synuclein); the strong fluorescence at the start of the unseeded experiment is likely to be due to an effect of SDS on ThT fluorescence. (*Inset*) The effect of SDS on the elongation of seed fibrils. The elongation kinetics of fibrils that were formed in the absence of SDS are very similar in the absence or presence of SDS.

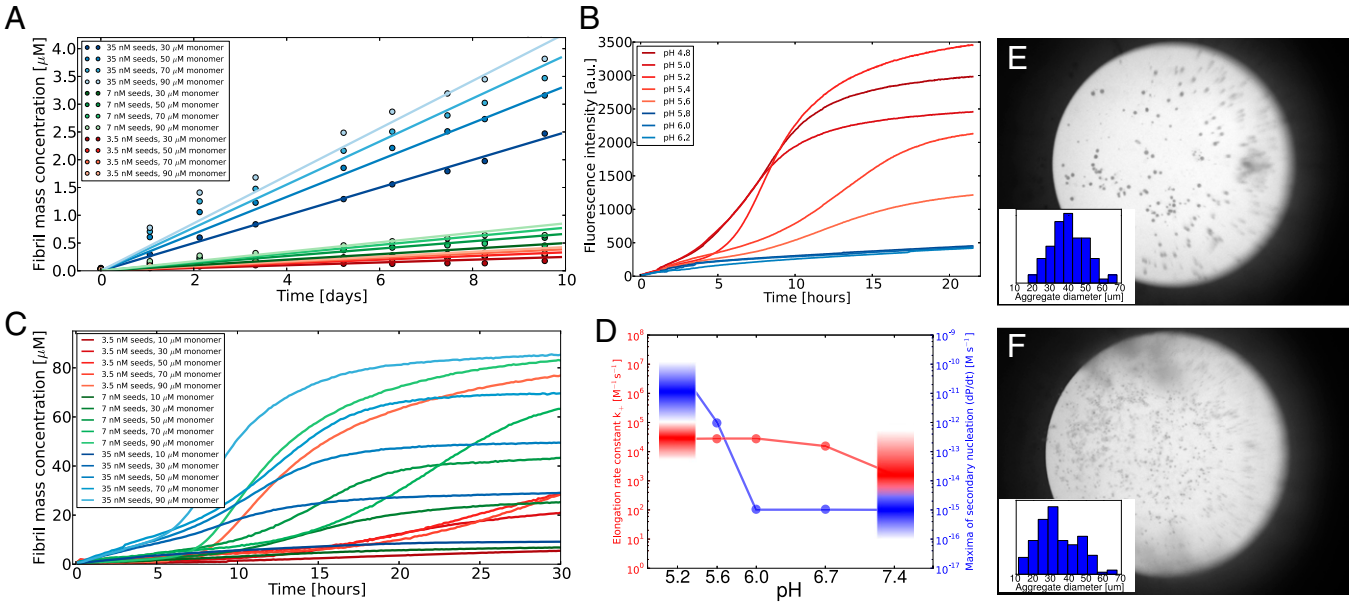

Fig. 4. The rates of the secondary nucleation processes in α-synuclein aggregation exhibit a dramatic pH dependence. (*A*) Growth of α-synuclein fibrils at very low seed concentrations in PBS buffer (pH 7.4, 45 °C, quiescent conditions). Both the seed and the monomer concentrations vary (*Inset*). A global fit is shown (continuous lines), considering only elongation, with two free parameters, the elongation rate constant k_+ and the saturation concentration for elongation, $m_{1/2}$. The fit yields $k_+ = 392\ M^{-1}{\cdot}s^{-1}$ and $m_{1/2} = 49.8\ \mu M$. (*B*) Seeded aggregation (50 μM monomer, 50 nM seeds, 10 mM PB, 37 °C, quiescent conditions) as a function of pH. (*C*) Experiments similar to those shown in *A*, but at pH 5.2 (10 mM PB, 37 °C, quiescent conditions), where significant secondary nucleation is observed. (*D*) Comparison of the elongation rate constant k_+ (red) and the maximal rate of fibril production through secondary nucleation (blue) at pH 5.2 (PB) and pH 7.4 (PBS), as well as an approximate indication of the pH dependence of both elongation and secondary nucleation. (*E* and *F*) Images (brightfield) of microwells at the end of the seeded experiment shown in *C* [10 μM monomer added at the beginning of the experiment, 3.5 nM seeds (*E*) and 35 nM seeds (*F*)]. Most of the ThT fluorescence is localized in the small assemblies of fibrils, the sizes of which have been determined and their distributions plotted as histograms.

datasets in Fig. 4 *A* and *C* that were acquired at low concentrations of seed fibrils were analyzed numerically (*SI Appendix*, section 13) and the maximal values for the quantity dP/dt, the rate of formation of new fibrils through secondary nucleation, was determined under those conditions. Fig. 4*D* shows a comparison of this quantity, as well as of the elongation rate constant, k_+, as a function of pH. Whereas the elongation rate constant changes by approximately one order of magnitude from pH 5.2 to pH 7.4 (*SI Appendix*, section 9), the rate of fibril production through secondary nucleation changes, quite remarkably, by at least four orders of magnitude.

Discussion

In this work, we have used aggregation assays in the presence of preformed seed fibrils to gain insight into various aspects of α-synuclein aggregation. First, we have measured the average elongation rate of mature α-synuclein amyloid fibrils under different conditions. From these experiments we have been able to determine the second-order rate constant for growth by monomer addition, k_+, to be *ca.* $2 \times 10^3\ M^{-1}{\cdot}s^{-1}$ at 37 °C in PBS buffer. This quantity has so far been determined for only a very few other amyloidogenic proteins in bulk solution; prominent examples include Aβ42 [$k_+ \sim 3 \times 10^6\ M^{-1}{\cdot}s^{-1}$ (4)] and a polyQ peptide with 23 glutamine residues [$k_+ \sim 10^4\ M^{-1}{\cdot}s^{-1}$ (36)]. This rate constant has also been determined from surface-based biosensor experiments for a range of proteins (37) and the results are generally in good agreement with the ones from the corresponding bulk solution experiments.

In addition to being able to elongate, α-synuclein fibrils are also subject to higher-order assembly processes that can be best described as flocculation followed by gelation of the protein aggregates (Movies S1–S10 show seeded experiments carried out in microcapillaries). These processes are strongly influenced by the salt concentration and therefore they are likely to be controlled by electrostatic interactions. Interestingly, the higher-order assembly of the growing fibrils strongly decreases their ability to seed aggregation. This effect most likely stems from a decrease in the effective diffusion rate of the soluble protein molecules and of the accessibility of the growth-competent ends under such conditions. Most of the experiments described in this paper were performed under quiescent conditions, which is likely to be more relevant to physiological behavior than experiments carried out under agitation, and is also simpler to interpret. We have found that under these conditions and at neutral pH values α-synuclein fibrils are not able to multiply at a significant rate. In agreement with other studies, however, we have shown that mechanical agitation can induce fragmentation of the fibrils (4, 38). By contrast, at mildly acidic pH (below pH 5.8), we have found that the same seed fibrils that were unable to multiply at neutral pH show strong signs of a secondary process giving rise to fibril proliferation even under quiescent conditions. Although such a change of ∼2 pH units increases the elongation rate constant by only approximately one order of magnitude, the production of new growing fibrils through secondary nucleation is enhanced by at least four orders of magnitude (Fig. 4*D*). The finding that the secondary process can be attributed to a surface-catalyzed process (*SI Appendix*, section 14 and Fig. 4 *E* and *F*) is consistent with the pH behavior that we have detected; its sharp pH dependence is most likely to be related to the titration of carboxylate groups in the acidic C terminus of the protein. *SI Appendix*, Fig. S12 shows the net charge of the protein, calculated as a function of pH, based on the pK_a values and Hill coefficients reported for 250 μM α-syn in 20 mM PB (39). Whereas the single histidine residue (H50) has a pK_a value of 6.8, the *ca.* 4.4 units calculated change in net charge between pH 6.0 and 5.0 is mainly due to the partial protonation of several carboxylate groups in the protein, especially in the acidic C terminus, which contains 16 carboxylate groups, 13 of which have elevated pK_a values (39). At lower protein concentrations and buffer strengths, as in the present study, as

well as in fibrils with many negative groups close together, these pK_a values are likely to be increased even more, in line with the salt dependence of α-synuclein pK_a values (39) and similar studies (40).

We conclude that the findings presented in this article may have significant implications for understanding the aggregation process of α-synuclein in vivo. It has been shown that the specific chemical microenvironments of cellular compartments, such as endosomes, can enhance protein aggregation by several orders of magnitude (41). Our study presents a physicochemical rationale for such effects in the case of the aggregation of α-synuclein. Our findings concerning the seeded aggregation of α-synuclein are likely to be of significant physiological importance, not just in the context of the primary growth of fibrils within cells that gives rise to Lewy bodies, but also in the context of the finding that healthy cells can be invaded by α-synuclein aggregates in a "prion-like" manner (42, 43), where aggregates spread to neighboring cells and accelerate the conversion of soluble protein molecules into fibrils and ultimately additional Lewy bodies. Such prion-like behavior can be explained by the existence of a secondary mechanism that is able to multiply existing aggregates, which can then be transmitted via diffusion or other means to neighboring cells. Our finding that such processes do indeed exist under quiescent conditions, and that they are very strongly influenced by the solution conditions, may help to explain the cellular localization as well as the kinetics and the mechanism of the spread of pathological aggregation in Parkinson disease.

Materials and Methods

Details can be found in *SI Appendix*. Wild-type human α-synuclein was recombinantly expressed and purified as described previously (12, 44). Seed fibrils were produced by incubating 500-μL solutions of α-synuclein at concentrations between 300 and 800 μM in 20 mM phosphate buffer at pH values between 6.3 and 7.4 for 48 to 72 h at *ca.* 40 °C. The increase in ThT fluorescence was monitored in low-binding, clear-bottomed half-area 96-well plates. Most experiments were performed under quiescent conditions, except for the experiments with added beads. Atomic force microscopy images were taken using a Nanowizard II atomic force microscope using tapping mode in air. The capillary experiments were performed in square borosilicate glass capillaries, which were monitored with an Observer D.1 inverted fluorescence microscope through a Filter set 47 using an Evolve 512 camera. The images of the wells after the aggregation were taken with an Olympus SZ61 stereomicroscope.

ACKNOWLEDGMENTS. We thank Georg Meisl for helpful discussions and Beata Blaszczyk for assistance with protein expression. This work was supported by the UK Biotechnology and Biological Sciences Research Council and the Wellcome Trust (C.M.D., T.P.J.K., and M.V.), the Frances and Augustus Newman Foundation (T.P.J.K.), Magdalene College, Cambridge (A.K.B.), the Leverhulme Trust (A.K.B.), the Swedish Research Council (E.S. and S.L.), the Swedish Foundation for Strategic Research (E.S.), the European Research Council (S.L.), and Elan Pharmaceuticals (C.M.D., C.G., T.P.J.K., and M.V.).

1. Otzen DE, ed (2013) *Amyloid Fibrils and Prefibrillar Aggregates: Molecular and Biological Properties* (Wiley-VCH, Weinheim, Germany).
2. Chiti F, Dobson CM (2006) Protein misfolding, functional amyloid, and human disease. *Annu Rev Biochem* 75:333–366.
3. Cohen SIA, Vendruscolo M, Dobson CM, Knowles TPJ (2012) From macroscopic measurements to microscopic mechanisms of protein aggregation. *J Mol Biol* 421(2-3):160–171.
4. Cohen SIA, et al. (2013) Proliferation of amyloid-β42 aggregates occurs through a secondary nucleation mechanism. *Proc Natl Acad Sci USA* 110(24):9758–9763.
5. Ferrone FA, Hofrichter J, Eaton WA (1985) Kinetics of sickle hemoglobin polymerization. II. A double nucleation mechanism. *J Mol Biol* 183(4):611–631.
6. Ruschak AM, Miranker AD (2007) Fiber-dependent amyloid formation as catalysis of an existing reaction pathway. *Proc Natl Acad Sci USA* 104(30):12341–12346.
7. Knowles TPJ, et al. (2009) An analytical solution to the kinetics of breakable filament assembly. *Science* 326(5959):1533–1537.
8. Cohen SIA, et al. (2011) Nucleated polymerization with secondary pathways. I. Time evolution of the principal moments. *J Chem Phys* 135(6):065105.
9. Conway KA, Harper JD, Lansbury PT (1998) Accelerated in vitro fibril formation by a mutant alpha-synuclein linked to early-onset Parkinson disease. *Nat Med* 4(11):1318–1320.
10. Fink A (2007) Factors affecting the fibrillation of α-synuclein, a natively unfolded protein. *Misbehaving Proteins: Protein (Mis)folding, Aggregation, and Stability*, eds Murphy R, Tsai A (Springer, Berlin), pp 265–285.
11. Giehm L, Otzen DE (2010) Strategies to increase the reproducibility of protein fibrillization in plate reader assays. *Anal Biochem* 400(2):270–281.
12. Grey M, Linse S, Nilsson H, Brundin P, Sparr E (2011) Membrane interaction of α-synuclein in different aggregation states. *J Parkinsons Dis* 1(4):359–371.
13. Jarrett JT, Lansbury PT, Jr. (1993) Seeding "one-dimensional crystallization" of amyloid: A pathogenic mechanism in Alzheimer's disease and scrapie? *Cell* 73(6):1055–1058.
14. Cohen SIA, Vendruscolo M, Dobson CM, Knowles TPJ (2011) Nucleated polymerisation in the presence of pre-formed seed filaments. *Int J Mol Sci* 12(9):5844–5852.
15. Ostwald W (1897) Studien über die Bildung und Umwandlung fester Körper. 1. Übersättigung und Überkaltung. *Z Phys Chem* 22:290–330.
16. Lomakin A, Chung DS, Benedek GB, Kirschner DA, Teplow DB (1996) On the nucleation and growth of amyloid beta-protein fibrils: Detection of nuclei and quantitation of rate constants. *Proc Natl Acad Sci USA* 93(3):1125–1129.
17. Kashchiev D, Auer S (2010) Nucleation of amyloid fibrils. *J Chem Phys* 132(21):215101.
18. Huang YY, Knowles TPJ, Terentjev EM (2009) Strength of nanotubes, filaments, and nanowires from sonication-induced scission. *Adv Mater* 21(38-39):39453948.
19. Sweers KKM, van der Werf KO, Bennink ML, Subramaniam V (2012) Atomic force microscopy under controlled conditions reveals structure of C-terminal region of α-synuclein in amyloid fibrils. *ACS Nano* 6(7):5952–5960.
20. Collins SR, Douglass A, Vale RD, Weissman JS (2004) Mechanism of prion propagation: Amyloid growth occurs by monomer addition. *PLoS Biol* 2(10):e321.
21. Lorenzen N, et al. (2012) Role of elongation and secondary pathways in S6 amyloid fibril growth. *Biophys J* 102(9):2167–2175.
22. Buell AK, et al. (2010) Frequency factors in a landscape model of filamentous protein aggregation. *Phys Rev Lett* 104(22):228101.
23. Serio TR, et al. (2000) Nucleated conformational conversion and the replication of conformational information by a prion determinant. *Science* 289(5483):1317–1321.
24. Giehm L, Svergun DI, Otzen DE, Vestergaard B (2011) Low-resolution structure of a vesicle disrupting α-synuclein oligomer that accumulates during fibrillation. *Proc Natl Acad Sci USA* 108(8):3246–3251.
25. Xue W-F, Homans SW, Radford SE (2008) Systematic analysis of nucleation-dependent polymerization reveals new insights into the mechanism of amyloid self-assembly. *Proc Natl Acad Sci USA* 105(26):8926–8931.
26. Wang C, Shah N, Thakur G, Zhou F, Leblanc RM (2010) Alpha-synuclein in alpha-helical conformation at air-water interface: Implication of conformation and orientation changes during its accumulation/aggregation. *Chem Commun (Camb)* 46(36):6702–6704.
27. Campioni S, et al. (2014) The presence of an air-water interface affects formation and elongation of α-Synuclein fibrils. *J Am Chem Soc* 136(7):2866–2875.
28. Zhu M, Li J, Fink AL (2003) The association of alpha-synuclein with membranes affects bilayer structure, stability, and fibril formation. *J Biol Chem* 278(41):40186–40197.
29. Necula M, Chirita CN, Kuret J (2003) Rapid anionic micelle-mediated alpha-synuclein fibrillization in vitro. *J Biol Chem* 278(47):46674–46680.
30. Ahmad MF, Ramakrishna T, Raman B, Rao ChM (2006) Fibrillogenic and non-fibrillogenic ensembles of SDS-bound human alpha-synuclein. *J Mol Biol* 364(5):1061–1072.
31. Pronchik J, He X, Giurleo JT, Talaga DS (2010) In vitro formation of amyloid from alpha-synuclein is dominated by reactions at hydrophobic interfaces. *J Am Chem Soc* 132(28):9797–9803.
32. Cremades N, et al. (2012) Direct observation of the interconversion of normal and toxic forms of α-synuclein. *Cell* 149(5):1048–1059.
33. Sasahara K, Yagi H, Sakai M, Naiki H, Goto Y (2008) Amyloid nucleation triggered by agitation of beta2-microglobulin under acidic and neutral pH conditions. *Biochemistry* 47(8):2650–2660.
34. Giehm L, Oliveira CLP, Christiansen G, Pedersen JS, Otzen DE (2010) SDS-induced fibrillation of alpha-synuclein: An alternative fibrillation pathway. *J Mol Biol* 401(1):115–133.
35. Eisenthal R, Cornish-Bowden A (1974) The direct linear plot. A new graphical procedure for estimating enzyme kinetic parameters. *Biochem J* 139(3):715–720.
36. Kar K, Jayaraman M, Sahoo B, Kodali R, Wetzel R (2011) Critical nucleus size for disease-related polyglutamine aggregation is repeat-length dependent. *Nat Struct Mol Biol* 18(3):328–336.
37. Buell AK, et al. (2012) Detailed analysis of the energy barriers for amyloid fibril growth. *Angew Chem Int Ed Engl* 51(21):5247–5251.
38. Xue W-F, Radford SE (2013) An imaging and systems modeling approach to fibril breakage enables prediction of amyloid behavior. *Biophys J* 105(12):2811–2819.
39. Croke RL, Patil SM, Quevreaux J, Kendall DA, Alexandrescu AT (2011) NMR determination of pKa values in α-synuclein. *Protein Sci* 20(2):256–269.
40. Kesvatera T, Jönsson B, Thulin E, Linse S (1996) Measurement and modelling of sequence-specific pKa values of lysine residues in calbindin D9k. *J Mol Biol* 259(4):828–839.
41. Hu X, et al. (2009) Amyloid seeds formed by cellular uptake, concentration, and aggregation of the amyloid-beta peptide. *Proc Natl Acad Sci USA* 106(48):20324–20329.
42. Kordower JH, Chu Y, Hauser RA, Freeman TB, Olanow CW (2008) Lewy body-like pathology in long-term embryonic nigral transplants in Parkinson's disease. *Nat Med* 14(5):504–506.
43. Desplats P, et al. (2009) Inclusion formation and neuronal cell death through neuron-to-neuron transmission of alpha-synuclein. *Proc Natl Acad Sci USA* 106(31):13010–13015.
44. Hoyer W, et al. (2002) Dependence of alpha-synuclein aggregate morphology on solution conditions. *J Mol Biol* 322(2):383–393.

SI Appendix: Solution conditions determine the relative importance of nucleation and growth processes in α-synuclein aggregation

Alexander K. Buell[1], Céline Galvagnion[1], Ricardo Gaspar[2], Emma Sparr[2], Michele Vendruscolo[1], Tuomas P.J. Knowles[1], Sara Linse[3] and Christopher M. Dobson[1,*]

[1]Department of Chemistry, University of Cambridge, Lensfield Road, Cambridge CB2 1EW, UK
[2]Department of Physical Chemistry, Lund University, SE221 00 Lund, Sweden
[3]Department of Biochemistry and Structural Biology, Lund University, SE221 00 Lund, Sweden
*author to whom correspondence should be addressed: cmd44@cam.ac.uk

Content

1 Materials and Methods

Reagents and chemicals

Thioflavin T (ThT), buffer salts, SDS and glass beads were purchased from Sigma (Gillingham, Dorset, UK). The 2 mm x 5 mm Teflon stir bars and 2 mm beads were purchased from Fisher Scientific (Loughborough, UK). Wild type human α-synuclein was recombinantly expressed and purified as described previously [1]. For concentration measurements, we used an extinction coefficient of 5600 M^{-1} at 275 nm. After the final size exclusion chromatography run (phosphate buffer, pH 6.5, 10-20 mM, depending on the intended experiment), the protein was snap frozen in liquid nitrogen in the form of 1 ml aliquots and stored at -80 °C. These aliquots were used without further treatment, except for the aggregation experiments at low pH, where an additional SEC run was performed on the thawed aliquots vs. 10 mM PB buffer at pH 4.8. The protein was then used directly. The pH was adjusted to the desired value with small volumes of 100 mM NaOH or HCl.
The concentration of soluble protein at the end of the aggregation assays was measured after ultracentrifugation of the samples for 45 min at 90 krpm. An absorbance spectrum was measured and corrected for the absorbance of ThT at 280 nm. Buffer solutions were degassed before use.

Seed fibril formation

Seed fibrils were produced by incubating 500 μl solutions of α-synuclein at concentrations between 300-800 μM in 20 mM phosphate buffer at pH values between 6.3 and 7.4, in the absence of added salt, for 48 - 72 h at ca. 40°C under maximal stirring with a Teflon bar on an RCT Basic heat plate (IKA, Staufen, Germany). The fibrils were distributed into aliquots, flash frozen in liquid N_2 and stored at -20°C until required. For aggregation experiments, the seed fibrils were diluted to 50-100 μM into water or the specific buffer to be used in the experiment and sonicated between 1 and 4 min using a probe sonicator (Bandelin, Sonopuls HD 2070), using 10% maximum power and 30% cycles.

Kinetic measurements of aggregation

The increase in ThT fluorescence was monitored in low binding, clear-bottomed half-area 96 well plates (Corning) that were sealed with metal sealing tape. We used Fluostar Optima, Polarstar Omega (BMG Labtech, Aylesbury, UK) and M1000 (Tecan group Ltd., Männedorf, Switzerland) fluorescence plate-readers in bottom reading mode. Most experiments were performed under quiescent conditions (no shaking), except for the experiments with added beads, where each reading cycle was followed by 300 s of shaking (linear shaking, 1mm amplitude). The simultaneous top- and bottom-optics experiments, as well as the spatially resolved absorption profile were performed with a Polarstar Omega platereader. The ThT concentration in the different experiments varied between 10 and 100 μM.

Data analysis

The data for the measurements of reproducibility were normalised by subtracting the fluorescence value at t = 0 and dividing the fluorescence intensity by its final value throughout the time course of the experiment. The dependence of the elongation rate on monomer concentration was determined by fitting the initial part of the curves to a linear function, rather than fitting the entire time course to an exponential or Lambert W function (see section 2). The reason for this difference in data analysis is twofold. First, a constant concentration of ThT was used in all samples and in the samples with highest monomer concentration, there is the possibility of depletion of the ThT towards the end of the timecourse. Second, the effects of flocculation of fibrils and their sedimentation is significant on time scales of hours (at low ionic strength), in particular for the samples with a high initial monomer concentration; therefore a restriction of the analysis to early times avoids this complication.

Analysis of fibril length disctributions

AFM images were taken using a Nanowizard II atomic force microscope (JPK, Berlin, Germany) using tapping mode in air. Fibril suspensions were diluted to below 1 μM in water and 10 μl were deposited on freshly cleaved mica and left to dry. The samples with the highest salt concentrations had to be rinsed carefully with water after the first drying and then were dried again. The length distributions were extracted with in-house written Python code, where the ends of the fibrils were manually selected.

Aggregation experiments in microcapillaries

We also performed real-time seeded aggregation experiments in square borosilicate glass microcapillaries with 0.5 mm inner diameter and 0.1 mm wall thickness. Using these capillaries, aggregation within confined spaces can be monitored at high spatial resolution and in the absence of an air-water interface. The experiments at high seed concentrations (videos S1-S6; to illustrate the flocculation) were performed at room temperature, and the experiments at low seed concentrations (videos S7-S10; to illustrate the secondary nucleation) were performed at 37°C. For the high seed concentration experiments, the concentration of soluble protein was ca. 100 μM and the seed concentration was 5 μM. The experiments at low seed concentrations (0.05-0.1 % of the concentration of monomeric protein) were also performed at lower monomer concentrations of ca. 50 μM. The capillaries were monitored during 1-3 h (high seed concentrations, 1 image per minute, 20x magnification) or 16 h (low seed concentrations, 1 image every 2 minutes, 10x magnification) through a Zeiss Observer D.1 inverted Fluorescence Microscope. The time courses of fluorescence intensity were extracted with in-house written Python software, that averages the fluorescence intensity over the entire area of the capillary. All movies were compressed with the open source software ffmpeg in order to allow easy upload.

Imaging of microwell plates after aggregation experiments

The higher order assembly of the growing seed fibrils can be visualized at low resolution at the end of an aggregation experiment through spatially resolved absorption measurements (see above). In order to obtain higher resolution optical information of the spatial distribution of aggregates, we took images of some of the microwells at the end of the experiments, in particular under conditions where secondary nucleation was observed. The images were taken with a Hamamatsu Orca 05G camera through a Olympus SZ61 stereo zoom microscope with bottom illumination.

2 The rate law for seeded growth of amyloid fibrils

In the limit of strong seeding, where other processes such as primary nucleation can be neglected, and under quiescent conditions, where fragmentation of fibrils is negligible, the differential equation for the consumption of soluble monomer is given by:

$$\frac{dm(t)}{dt} = -k_+ P(t) m(t) \tag{1}$$

where m(t) denotes the monomer concentration, k_+ the molecular rate constant of fibril elongation, and $P(t)$ the number concentration of fibrils (or rather growth-competent ends). If $P(t) = \text{const} = P(0)$ (negligible primary and secondary processes), this equation can be simplified to:

$$\frac{dm(t)}{dt} = -k_{+,\text{eff}} m(t) \tag{2}$$

where $k_{+,\text{eff}} = k_+ P(0)$. Neglecting the initial seed concentration (the initial fluorescence was subtracted from all curves for the analysis), the solution to this equation with the initial monomer concentration $m(0)$ is given by $m(t) = m(0)e^{-k_{+,\text{eff}}t}$. In the experiments described in this work, we measure the increase in fibrillar mass concentration (via an increase in ThT fluorescence), rather than the decrease in monomer concentration. Therefore the normalized expression for the observed increase in fibrillar mass $M(t)$, using $M(t) + m(t) = m(0)$ is given by:

$$\frac{M(t)}{m(0)} = 1 - e^{-k_{+,\text{eff}}t} \tag{3}$$

This simple description, however, has to be modified if the initial monomer concentration is significantly higher than the turnover concentration: $m(0) > m_{\frac{1}{2}}$. As we show in this study, the consumption of soluble protein by elongation of α-synuclein fibrils, rather than depending linearly on the monomer concentration, is of the functional form:

$$\frac{dm(t)}{dt} = -\frac{k_{+,\text{eff}} m_{\frac{1}{2}} m(t)}{m(t) + m_{\frac{1}{2}}} \tag{4}$$

which has been shown to describe the saturation of the elongation rate at high monomer concentration observed for other amyloid systems [2], and where $\text{m}_{\frac{1}{2}}$ denotes the concentration at which the elongation rate has reached half of its limiting maximal value. This expression has the limits $\lim_{m\to+\infty} \frac{dm(t)}{dt} = -k_{+,\text{eff}} m_{\frac{1}{2}} = \text{const}$ and $\lim_{m\to 0} \frac{dm(t)}{dt} = -k_{+,\text{eff}} m(t)$. This more general expression can also be integrated with $m(0)$ as the monomer concentration at time 0 and yields the following expression:

$$m(t) = m_{\frac{1}{2}} \text{W}\left(\frac{e^{\frac{m(0)}{m_{\frac{1}{2}}} - k_{+,\text{eff}} t} m(0)}{m_{\frac{1}{2}}} \right) \tag{5}$$

where W denotes the Lambert W (or product log) function, which is defined through the equation $z = \text{W}(z)e^{\text{W}(z)}$ for any $z \in \mathbb{C}$.

SI Appendix Figure 1 shows a comparison of fits to an elongation curve acquired at $m(0)$=70μM. This starting monomer concentration is larger than $\text{m}_{\frac{1}{2}}$ determined in this work (45±5μM). However, the comparison of the fits shows that the simple exponential model describes the data better, therefore suggesting that in practical terms, the exponential model can be used as long as m_0 is not much larger than $m_{\frac{1}{2}}$. We therefore performed the global fit in Figure 3 in the main manuscript, as well as the fits shown in Figures 3, 4 and 6 in the SI Appendix using the exponential model. However, in Figure 4 in the main manuscript, inclusion of the sub-linear concentration dependence of the elongation rate into the fit was necessary, due to the fact that concentrations up to 90 μM were measured.

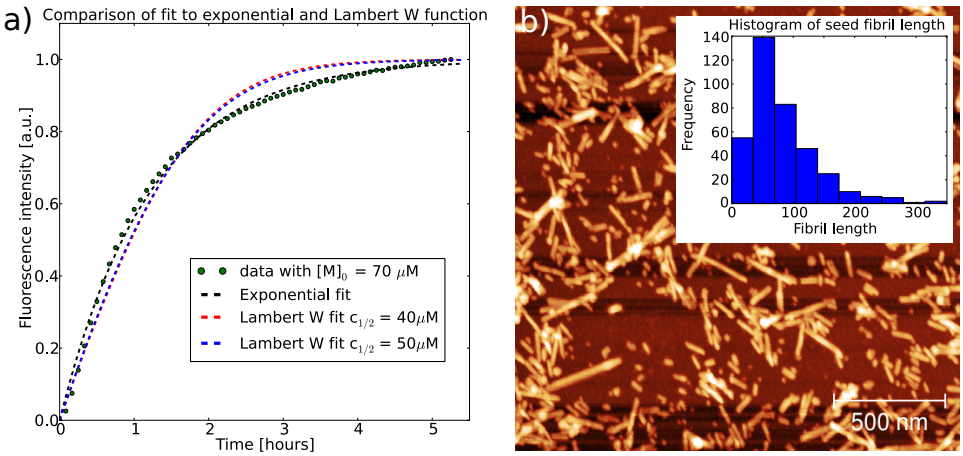

Figure 1: a) Comparison of a fit to a simple exponential function with a fit to Lambert W functions ($m_{\frac{1}{2}}$=40μM and 50 μM) of one of the data sets of the section below. Despite the fact that the starting monomer concentration $m(0)$ = 70 μM> $m_{\frac{1}{2}}$, the data is better described by the exponential function. b) AFM image of sonicated seed fibrils, together with the corresponding histogram of the fibril length distribution.

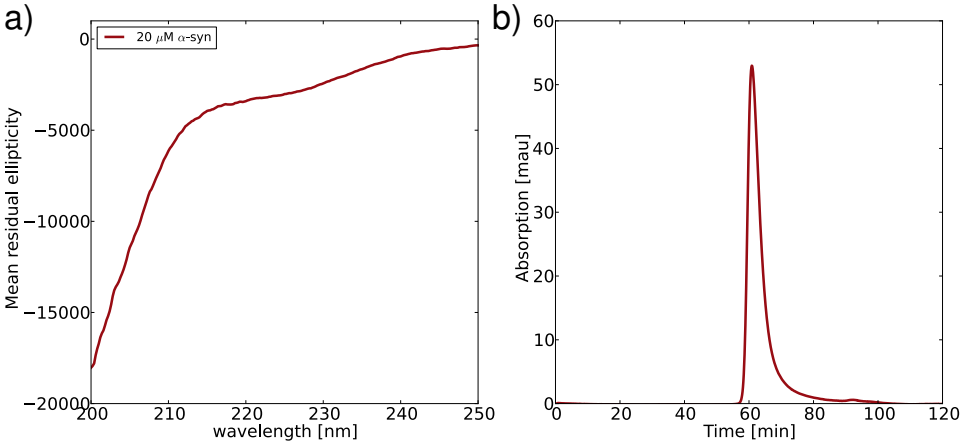

Figure 2: a) Far UV circular dichroism (CD) spectrum demonstrating the random coil character of the soluble, monomeric α-synuclein used in in our seeded aggregation experiments. b) Size exclusion chromatogram of the last step in the purification of α-synuclein. In this case, the protein is eluted in 10 mM PB pH 5.5.)

Rather than using the value for $m_{\frac{1}{2}}$ determined from the experiment shown in Figure 2 in the main manuscripts, we allowed $m_{\frac{1}{2}}$ to vary in the fit. This data was not fitted to Lambert W functions, but rather to a set of linear functions, as at these extremely low seed concentrations, only a small fraction of the total available monomer is converted into fibrils and therefore the linear approximation is a good description for both the exponential and Lambert W functions.

3 α-synuclein is monomeric under the solution conditions used in our experiments

In the last three years, since the report by the Selkoe group [3] that α-synuclein occurs naturally as a folded α-helical tetramer, the structure of soluble α-synuclein has been controversially discussed. The question whether α-synuclein is indeed in some cases tetrameric *in vivo* has not been finally answered; however, most available biophysical characterizations of α-synuclein *in vitro* [4] as well as *in vivo* [5] and also in a recent study of *ex vivo* [6] protein are consistent with the occurrence of α-synuclein as a monomeric intrinsically disordered protein in solution. We have performed circular dichroism (CD) spectroscopy of the soluble α-synuclein (SI Appendix Figure 2 a) and we find that the CD spectrum of the protein is consistent with a disordered, rather than an α-helical state.

We also show a typical size exclusion chromatogram of the last step in the purification of α-synuclein (SI Appendix Figure 2 b), demonstrating the monodisperse character of the protein at this stage of the preparation.

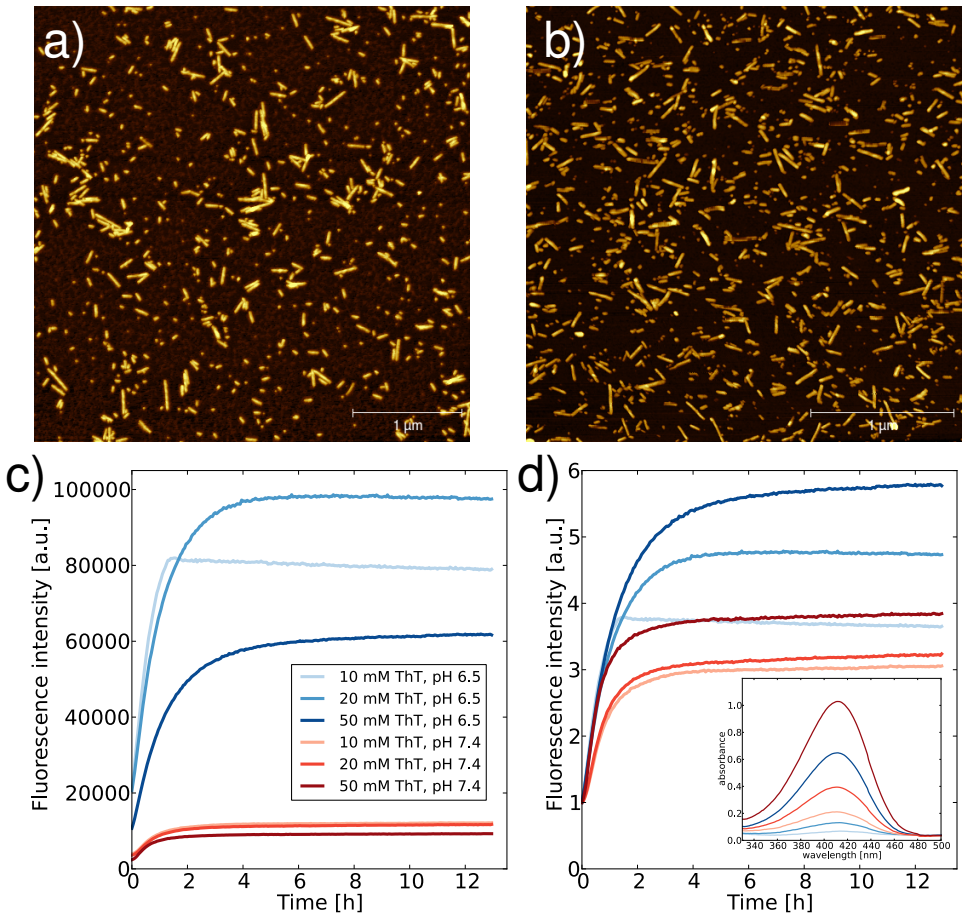

Figure 3: Fibrils formed in a) 20 mM PB at pH 6.3 (mean length 79.5 nm) and b) 20 mM PB at pH 7.4 (mean length 85.6 nm), sonicated in both cases for a total of 70 s. c) Raw data of kinetic experiments (50 μM) monomer, 2.5 μM seeds, 20 mM PB buffer at same pH under which the fibrils had been formed. d) Kinetic data normalized to the fluorescence value at t = 0 of the 10 μM ThT sample for both fibril types separately. The inset to d) shows absorbance spectra of the supernatant of the reaction mixtures at the end of the fibril elongation.

4 The influence of solution conditions on the properties of the formed seed fibrils

It has recently been reported that different solution conditions, such as changes in salt concentrations, can induce the formation of different strains of α-synuclein amyloid fibrils [7]. In the present study, we have produced seed fibrils in the absence of added salt, as the higher order association and gelation of the fibrils (see below for a detailed description) is strongly enhanced by increased ionic strength, interfering with the quantitative conversion of the protein into amyloid fibrils desirable for the formation of seed fibrils. Here, we have formed amyloid fibrils of α-synuclein under different pH-conditions, in particular pH 7.4 and at slightly more acidic pH, 6.3-6.5. SI Appendix Figures 3 a) and b) show that the morphologies of the fibrils are very similar. However, we noticed that the fibrils formed under these different conditions exhibit differences in the affinity for Thioflavin T (ThT). SI Appendix Figure 3 c) shows kinetic data of seeded experiments for both types of seed fibrils under the pH conditions where the fibrils had been formed, at 3 different ThT concentrations. It can be seen that both the shapes of the curves and the absolute fluorescence intensities depend on the ThT concentrations. Interestingly, the lowest ThT concentrations yield the highest fluorescence intensity values. This phenomenon is likely to be linked to the micellisation of ThT that has been reported previously [8], and a potential fluorescence self-quenching effect caused by the micelle formation. When the fluorescence intensity values are normalized to the value at t = 0 (see SI Appendix Figure 3 d), these effects can be more easily compared.

Whereas 10 μM ThT is sufficient in the case of the fibrils made at pH 7.4, ThT concentrations in excess of 20 μM should be used in the case of seed fibrils formed at pH 6.3. In the remaining experiments described in this work, we have consistently used seed fibrils formed at pH values between 6.3 and 6.5 at concentrations in excess of 500 μM. As can be seen in SI Appendix Figure 3, these fibrils yield very high fluorescence intensity values, which renders experiments

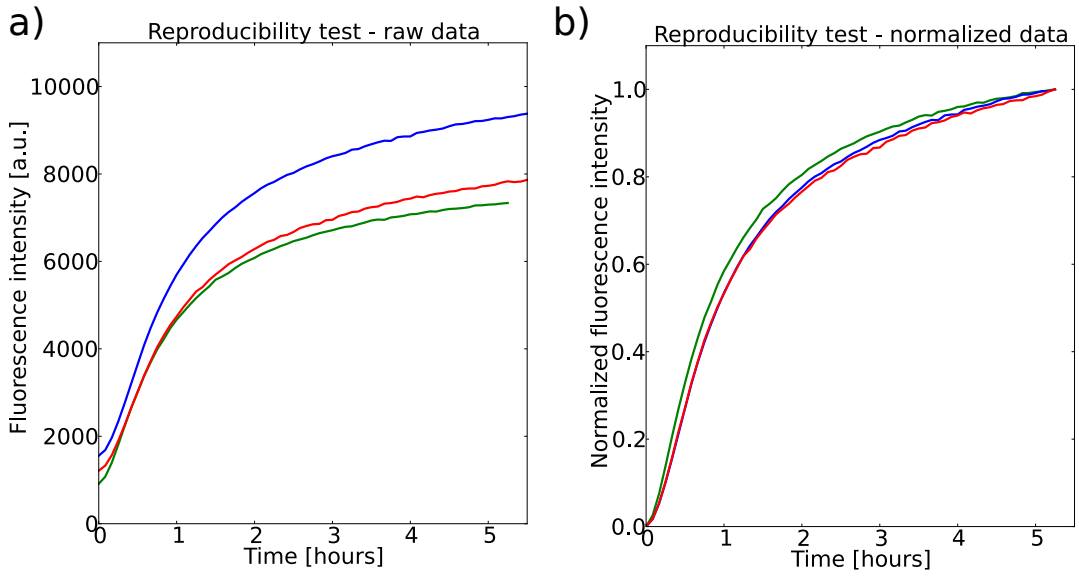

Figure 4: a) Exploration of the reproducibility of the seeded aggregation assay. Three experiments are illustrated where, in each case, a different batch of seed fibrils was used. The experiments were performed with identical settings of the plate-reader and the same concentrations of soluble protein (70 μM) and Thioflavin-T (100 μM). b) When the data are normalised (see Methods) the agreement between the independent experiments is very good; the fitted exponential constants are 0.825 h^{-1}, 0.735 h^{-1}, 0.720 h^{-1}.

at exceedingly low seed concentrations easier, such as the ones shown in Figure 3 of the main manuscript. In order to reliably follow the fluorescence time courses of elongation of these fibrils, we therefore used ThT concentrations of 50 μM or above.

5 Reproducibility of seeded aggregation with well-defined ensembles of seed fibrils

In order to demonstrate the exceptional reproducibility of fibril growth kinetics that can be obtained from such an approach, we produced seed fibrils at pH 6.5 from three different batches of α-synuclein (see Methods section for details), and incubated them at 45°C in PBS buffer containing 70 μM monomeric protein. The raw data from the three independent experiments are shown in the inset to SI Appendix Figure 4 a) and reveal that, although the absolute fluorescence values vary by up to 25%, upon normalisation (see Methods) the traces are virtually superimposable. Independent fits to single exponential functions of the form $1 - e^{-kt}$ of the normalised data (see Section 2) give values of the apparent rate constant k that are within 15% of each other (0.76±0.06 h^{-1}; see legend to SI Appendix Figure 4 b).

6 The concentration-dependence of α-synuclein amyloid fibril growth

During our experiments with seed fibrils formed under different conditions, we noticed that the saturation behaviour of the elongation rate as a function of the concentration of soluble protein depended on the nature of the seed fibrils. Most of the experiments in this work were performed with seed fibrils formed at pH 6.3-6.5 and the fitted values for the monomer concentration at which half the maximum rate is reached, $m_{\frac{1}{2}}$, are consistent between for example the data sets shown in Figure 2 a) and Figure 4 a) of the main manuscript, where the seed fibrils were elongating under very similar conditions. However, we found that in some cases, the linearity of the elongation rate as a function of soluble protein concentration extended to higher concentrations. In SI Appendix Figure 5, we have plotted equivalend experiments, where seed fibrils, that had been formed under different conditions (PBS, stirring and 10 mM MES buffer, pH 5.5, quiescent in polystyrene coated microwell plates) were left to elongate in PBS. In these cases, a fit of the data to a function of the form $r(m) = \frac{k_{+,\mathrm{eff}} m_{\frac{1}{2}} m}{m_{\frac{1}{2}} + m} = \frac{r_{max} m}{m_{\frac{1}{2}} + m}$, [2] yields values of $m_{\frac{1}{2}}$ several fold larger than those reported

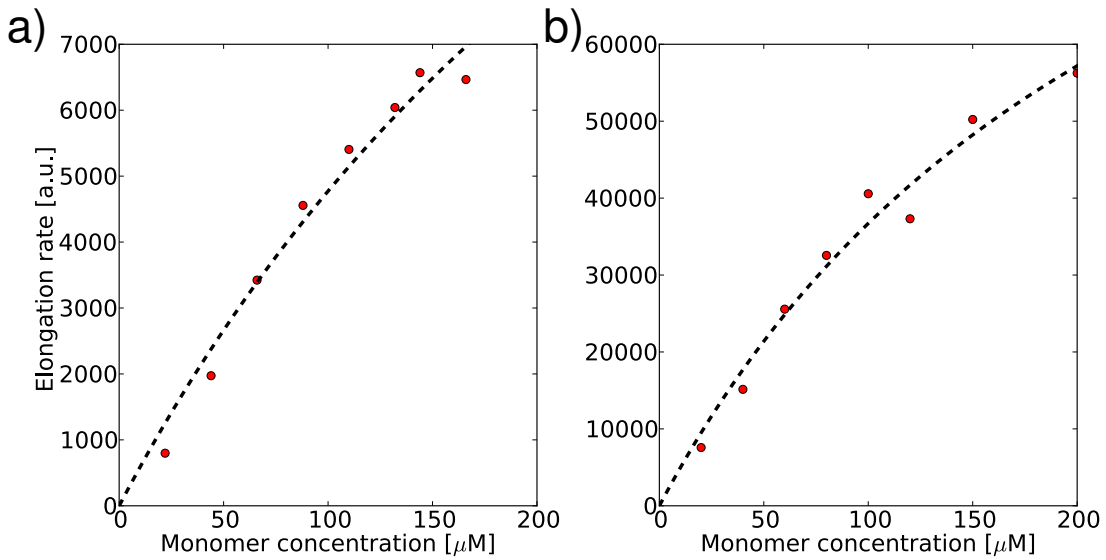

Figure 5: The dependence of the elongation rate on the concentration of soluble protein for different seed fibrils a) Seed fibrils formed in PBS buffer ($m_{\frac{1}{2}} = 380$ μM) b) Seed fibrils formed in MES buffer pH 5.5 in polystyrene coated plates [9] ($m_{\frac{1}{2}} = 250$ μM).

in the main manuscript. We do not currently know whether this result suggests a true dependence of the quantity $m_{\frac{1}{2}}$ on the structure of the seed fibrils, or whether it is influenced by other factors, such as the higher order assembly of the fibrils. We note, however, that the data is in all cases consistent with a saturation at higher concentrations of soluble protein, and therefore with fibril elongation by monomer addition.

7 The temperature-dependence of α-synuclein amyloid fibril growth

One of the most basic parameters that can be varied, and that can provide insight into the mechanism of the reaction, is the temperature at which the reaction is carried out. For a determination of the temperature-dependence, which allows the enthalpic part of the free energy barrier of fibril elongation to be measured [10], we carried out seeded fibril growth experiments at four different temperatures (30, 35, 40 and 45°C) using the same batch of seed fibrils, and four fluorescence plate readers operating in parallel (SI Appendix Figure 6).

We then normalised the data, and analysed it in two different ways: fitting exponential functions to the individual time courses and using the rate constants to generate an Arrhenius plot, as well as performing a global fit to the entire set of four curves with only two parameters: the effective rate constant at 30°C and the enthalpy of activation $\Delta H^{\ddagger}$. Both fits are shown in SI Appendix Figure 6, and the values for $\Delta H^{\ddagger}$ show a very high degree of consistency (52.6±3.2 and 52.7±0.5 kJ/mol). In agreement with literature reports [10–12], we find a non-negligible enthalpic barrier, demonstrating that fibril elongation is an activated process where a range of interactions needs to be broken before the system can reach the transition state. The value of $\Delta H^{\ddagger}$ determined here is ∼25% lower than the value that we have previously reported for α-synuclein and that was obtained from surface-based biosensing [10]. This difference is surprising in the light of our recent results that show that for example the effect of changes in ionic strength on the kinetics of amyloid fibril growth is indistinguishable for surface-attached fibrils or fibrils in bulk solution [13]. In addition, for the elongation of insulin amyloid fibrils, it has been shown that the temperature dependencies in bulk solution [14] and on a surface [15] are very similar. The difference in this case could stem from the fact that additional interactions between the soluble α-synuclein and the surface exist that increase the overall enthalpy of activation for the growth of surface-bound fibrils. It is more difficult to compare the value of $\Delta H^{\ddagger}$ determined here with the values reported in an earlier solution-based study [11], as in this case, the temperature-dependence of the slope in an un-seeded experiment was probed, which has been shown to contain contributions from processes other than fibril elongation [16].

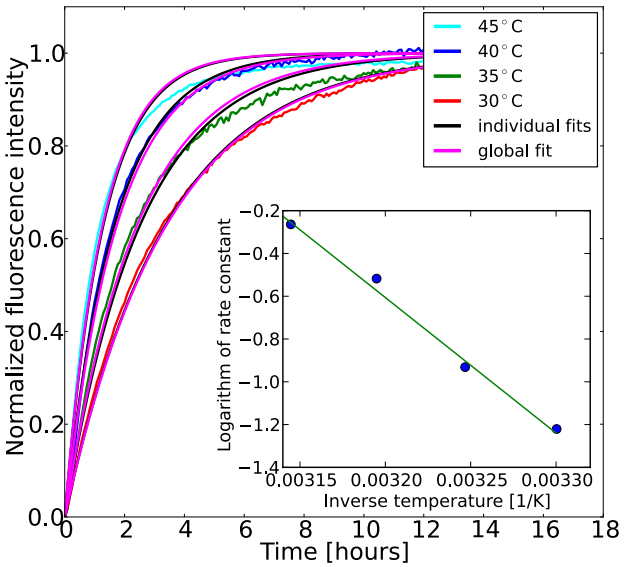

Figure 6: The temperature dependence of seeded aggregation was probed in the range 30-45°C. The data were fitted in two ways; as a global fit with $k_{+,\mathrm{eff}}$ and $\Delta H^{\ddagger}$ as free parameters and as independent fits to the four curves. The inset shows an Arrhenius-plot of the rate constants from the latter fit, that yields an enthalpy of activation $\Delta H^{\ddagger}$ of 52.6±3.2. The global fit yields $\Delta H^{\ddagger}$ = 52.7±0.5 kJ/mol.

8 Determination of (ensemble) absolute elongation rates under different conditions

The elongation of pre-existing seed fibrils, as investigated and discussed in detail in this work, increases only the total mass of aggregates, while keeping the number constant. Therefore, in order to be able to determine the absolute rate of fibril elongation, only the initial number concentration of seed fibrils has to be known. We determined the fibril length distribution by atomic force microscopy; AFM images of sonicated fibrils are shown in SI Appendix Figure 3 a) and b) and in Figure 1 b), where a histogram of fibril lengths is also shown (See Section 1 for details). Taking the mean fibril length as the measured value of 83±54 nm (SI Appendix Figure 1 b) and an observed average fibril thickness of 7±2 nm (also from AFM imaging), we calculate an average number of monomers per seed fibril of ∼180 ($\rho_{\alpha syn}$ = 1.35 g/cm^3 [17], M$_{\alpha syn}$ = 14.5 kDa).

In order to get a robust estimate of the absolute elongation rate, we used the result of a global fit of the data set shown in Figure 2 in the main manuscript. Here, the monomer concentration at the start of the experiment was m_0 = 50 μM and the seed (mass) concentration varied between 1 and 0.05 μM. For comparability with the analysis in section 11, we performed a global fit to the Lambert W model, using the mean number of monomers per seed fibril determined above, and assuming that all fibrils grow from both ends. We obtain as average elongation rate constant under these conditions (37°C, PBS buffer): k$_+$ = ∼2200 M^{-1}s^{-1}. This value is approximately one order of magnitude lower than the value that we have reported previously for the same quantity under similar solution conditions and that was determined from surface-based biosensing [10]. This difference can be partly explained through the fact that in solution based measurements, the molecular rate constant will be an average over all seed fibrils, whereas in the surface-based sensing experiments, it is easier to estimate the fraction of seeds that have contributed to the conversion of monomer [10]. It is interesting to translate the molecular rate constants of fibril growth into absolute length increase of the fibrils. At 37°C and 20 μM soluble protein concentration, α-synuclein fibrils grow on average 1-2 nm/min in PBS buffer (assuming a fibril diameter of 7 nm, and using the value of k_+ determined here).

In order to gain some insight into the dependence of the elongation rate on the solution conditions, we have performed experiments in dilute phosphate buffer in the absence of added salt (SI Appendix Figure 7). We find that the elongation rate constant is relatively pH-independent for pH values up to 6, but then decreases by about one order of magnitude at pH 7.3. A fit to the data at pH 6.1 yields k$_+$ = ∼30000 M^{-1}s^{-1}.

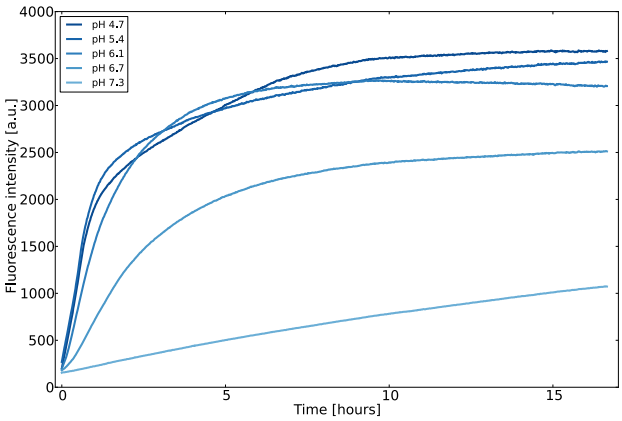

Figure 7: The pH-dependence of α-synuclein amyloid fibril elongation in 10 mM PB, 37°C under quiescent conditions. The monomer concentration is 45 μM and the seed concentration is 2.5 % by mass. All experiments were performed with the same batch of seed fibrils, formed at pH 6.3.

9 Variation of seeding efficiency with sonication duration

In order to gain additional insight into the effect that probe sonication (see Section 1) has on the seeding efficiency of α-synuclein fibrils, we have compared the length distributions and seeding efficiencies of seed fibrils after different sonication times. The results are shown in SI Appendix Figure 8. One minute of sonication leads to a decrease of the mean fibril length by a factor of 2.6, whereas the seeding efficiency, determined as the effective rate constant of a fit to a single exponential function, and a measure for the number of growth competent ends, only increases by a factor of 1.6. We conclude that it is likely that part of the newly created fibril ends are not capable of acting as growth sites. This phenomenon may be due to the strong heating that is induced by the sonication. It is difficult to quantify this effect more accurately without extensive systematic analysis of length distributions by AFM; however, we note here that as our calculations of the molecular rate constant are based on the assumption that all seed fibrils can grow, the absolute value of the molecular rate constant per growing fibril will increase if only part of the fibrils grow.

10 Higher order assembly of α-synuclein amyloid fibrils

It has been reported previously that α-synuclein fibrils can associate into higher order aggregates under conditions where electrostatic repulsions between fibrils are decreased, i.e. at pH values close to the isoelectric point of the protein [1]. However, the effect of this process on aggregation kinetics has so far not been considered. We have performed seeded experiments in PBS buffer at physiological ionic strength values where electrostatic interactions are very short range [18] (see Figure 2 in the main manuscript) and in 20 mM phosphate buffer (PB, see SI Appendix Figure 9 a). We show here that the higher order assembly of amyloid fibrils can affect both the absolute kinetics of aggregation, as well as the solution-based measurements discussed in this work. SI Appendix Figure 9 a) shows the result of an experiment where the seed concentration was systematically varied, similar to the data shown in Figure 3 a) in the main manuscript. As in the case of PBS, the fit describes the overall increase in ThT fluorescence well. In addition, the shapes of the individual curves resemble more closely single exponential functions; in particular the deviations between the data and the fits at early times are lower than in the case where PBS was used as a buffer.

The observation that the ThT fluorescence signal increases faster at early times than predicted if only fibril elongation occurred in the system could in principle have two origins. It could indicate the origin of secondary pathways that increase the number of fibrils and therefore accelerates the reaction, or it could be due to a process that leads to enhanced measured signal without a true accelerated increase in total aggregate mass. As all the experiments were performed with bottom optics, sedimentation of aggregates of fibrils towards the optical head would yield precisely this effect. In order to probe this hypothesis, we performed a ThT fluorescence experiment where we measured simultaneously the increase in fluorescence with top- and bottom-optics both in the presence of 20 mM PB and PBS (SI Appendix Figure 9 b). We found that while in the presence of 20 mM PB the normalised (by initial value) curves are virtually superimposable, indicating negligible sedimentation over a timescale of several hours, we find a strong divergence in the rate of change of fluorescence intensity for the sample with PBS buffer. Indeed the top optics do not detect the substantial increase in ThT fluorescence measured by the bottom optics. These results give strong support for the hypothesis that the deviations from single exponential kinetics at early times are due to higher order assembly of fibrils and their subsequent sedimentation. It is interesting to note that the timescale over which a difference in top-

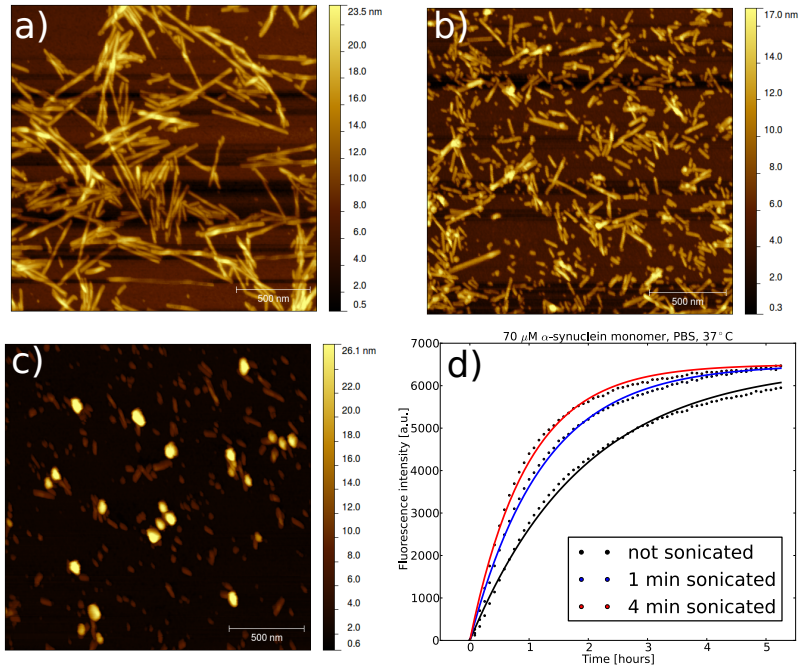

Figure 8: In order to test whether probe sonication renders some seed fibrils inactive, we have acquired AFM images of α-synuclein fibrils after 48h of stirring (a), and additional 1 min (b) and 4 min (c) of probe sonication (for details see Methods section of main manuscript). We have determined the mean lengths to be 216, 83 and 57 nm respectively. We also compared the seeding efficiencies of fibrils prepared in this way (d) and found the effective rate constants to be 0.52 s^{-1}, 0.82 s^{-1} and 1.04 s^{-1}. Therefore the seeding efficiency increases less strongly than expected from the shortening of the length distribution, indicating some loss of active ends due to the probe sonication.

and bottom reading is observed for the PBS sample requires aggregate sizes of the order of μm. Equating gravitational and friction forces, $\frac{4}{3}\pi R^3 \Delta\rho g = 6\pi\eta R\nu$, where R is the radius of a sphere that moves with velocity ν in a fluid with viscosity η and $\Delta\rho \approx 0.2 g/cm^3$ is the difference in density between protein and water, we compute that a protein aggregate with an effective radius of 1 μm sediments under the action of gravity at a rate of 0.4 mm in 10 min, a value of the right order of magnitude to explain the observed effect. We conclude that at high ionic strength values, amyloid fibrils formed from α-synuclein form a highly unstable colloidal suspension that aggregates very rapidly into structures of the order of μm. This phenomenon can be illustrated through a comparison of the spatially resolved absorption profile at 450 nm (close to the absorption maximum of bound ThT) of microwells at the end of the aggregation reaction with both 20 mM PB and PBS (SI Appendix Figure 9 c and d). While the content of the PB well is macroscopically homogeneous, large aggregates can be detected in the wells with PBS.

In order to visualize the flocculation and gelation of the growing fibrils in real time, we have also performed aggregation experiments at high seed and monomer concentrations in glass microcapillaries (see SI Appendix section 1 for experimental details). The corresponding videos can be found as additional SI (videos S1-S6). We have performed these experiments with two different types of seed fibrils, formed at pH 6.3 and pH 7.4. Interestingly, we find that not only the solution conditions (mainly the total concentration of buffer- and added salts) determine the propensity for higher order aggregation, but also the nature of the seed fibrils. Most of the videos (unless stated otherwise in the filename) are of experiments performed with seed fibrils produced at pH 6.3. When those fibrils are let to elongate at pH 6.3 in the presence of a high concentration of soluble α-synuclein, development of spatial inhomogeneity can be observed to an increasing degree in the followings sequence of solution conditions: 10 mM PB (pH63_lowI_highseed_comp.avi), 20 mM PB (pH63_highseed_comp.avi), 20 mM PB + 150 mM NaCl (pH63_150mMNaCl_highseed_comp.avi), 20 mM PB + 50 mM $CaCl_2$ (pH63_50mMCaCl2_highseed_comp.avi). In particular, 50 mM $CaCl_2$, which has formally the same ionic strength as 150 mM NaCl leads to a much more rapid and pronounced flocculation, indicating specific ion effects rather than just a Debye screening at the origin of the effect. If the experiments are performed with seed fibrils formed at pH 7.4, on the other hand, no significant higher spatial inhomogeneities are observed in 20 mM PB at pH 6.3 (pH63_pH74seeds_highseed_comp.avi). However, the seeds formed at pH 7.4 do show flocculation when they are left to elongate in the presence of 150 mM NaCl at pH 7.4 (pH74_150mMNaCl_pH74seeds_highseed_comp.avi). Therefore, the surface properties of the seed fibrils seem to not only depend on the conditions in which they are left to elongate, but also to some extent on the conditions under which they have been formed, as also suggested by their different

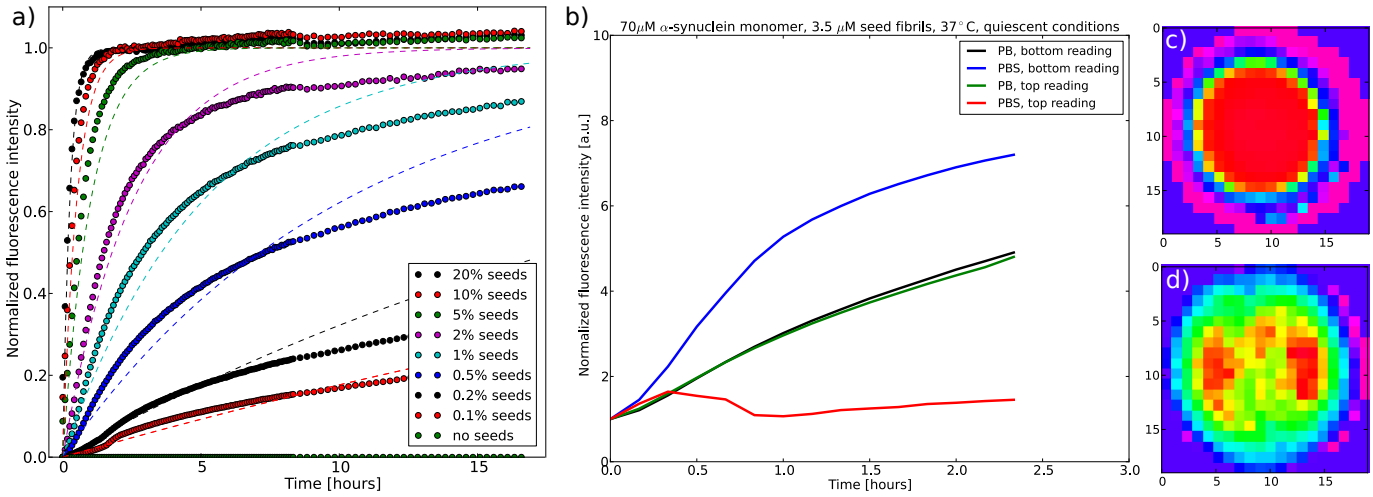

Figure 9: a) Seeded experiments with decreasing seed concentration, similar to the ones shown in Figure 3 a) of the main manuscript, were performed in 20 mM PB (60 μM soluble protein, 45°C, pH 6.4) in order to probe whether higher order assembly of fibrils can explain the deviation from simple exponential behaviour observed for the data acquired in PBS. The temperature was increased in order to accelerate the growth, which can be expected to reduce the relative importance of fibril assembly. Indeed, the global fit to a model that exclusively takes elongation into account is significantly better than in the case where PBS was used as buffer solution and where the total ionic strength is of the order of 150 mM. b) Time-course of seeded aggregation of α-synuclein in 20 mM PB and in PBS, where the change in ThT fluorescence has been measured with top and bottom optics simultaneously. The data has been normalised to the initial fluorescence value. In the case of PB, the traces superimpose, indicating that sedimentation of higher order aggregates of fibrils is not significant and that the sample is spatially homogeneous. However, in PBS buffer, the traces of bottom- and top-reading start to diverge almost from the start. Sedimentation of fibrils, which removes them from the optical fibre, even overcomes the increase of fluorescence intensity due to the growth of the fibrils. c) and d) Spatially resolved absorbance at 450 nm in the wells of a micro-well plate where a seeded aggregation experiment had been carried out in c) PB 20 mM and d) PBS. The absorbance is more inhomogeneous in the case of PBS, demonstrating the macroscopic assembly of fibrils to form large scale aggregates. These results demonstrate the importance of electrostatic screening for the higher order assembly of α-synuclein fibrils.

affinities to ThT (see SI Appendix section 4).

11 Decrease in seeding efficiency due to higher order association of fibrils

The data shown in Figure 2 of the main manuscript are overall well described by an elongation-only-model. The observation that data from longer experiments (Figure 4 of main manuscript) are in better agreement with a model that only considers elongation compared to data acquired at higher seed concentrations could stem from the fact that the higher order association ("flocculation") of fibrils and subsequent sedimentation (see above) operates on a timescale of minutes to hours. In experiments significantly longer than the characteristic timescale of these processes, the system of elongating and associating fibrils is in (gravitational) equilibrium and hence the spatially inhomogeneous distribution of growing aggregates does not distort the aggregation time course. However, as higher order association of fibrils is likely to decrease the number of accessible fibril ends, the average elongation rates of such long-time experiments should be lower than the corresponding elongation rates (scaled by fibril concentration) in shorter experiments (such as the one shown in Figure 2 in the main manuscript). This hypothesis can be tested by comparing the result of a global fit to the data at low seed concentration (Figure 4 a in the main manuscript) with the elongation rate constant determined at high seed concentration (see Section 8). As discussed above, we obtain for the latter $k_+ \approx 2200$ $M^{-1}s^{-1}$, whereas the global fit in Figure 4 a) in the main manuscript (with k_+ and $m_{\frac{1}{2}}$ as free parameters) yields $k_+ \approx 390$ $M^{-1}s^{-1}$, assuming the same fibril length distribution. We can use the temperature dependence determined above to correct for the fact that the data in Figure 2 were measured at 37°C and the data in Figure 4 at 45°C. We finally obtain an elongation rate constant of $k \approx 230$ $M^{-1}s^{-1}$, almost an order of magnitude lower than the one determined at higher seed concentration. The difference between those values is therefore most likely to be due to a several fold decrease in the number of growing ends caused by higher order association of fibrils.
In this context, it is interesting to note that, despite the sigmoidal reaction profile of the weakly seeded reactions in

the presence of the beads (Figure 3 in main text), the reaction is not complete when the plateau of the fluorescence is reached; when the reaction mixture is centrifuged (see Methods), it is found that significant amounts of soluble protein (∼60% of the initially added monomer) are left. This finding is further evidence for the higher order assembly of fibrils discussed above, that this assembly is not prevented by agitation of the sample, and that it strongly decreases the efficiency of the seeding process. It is likely that similar processes are at the origin of the high values that have been reported in the past for the concentration of soluble α-synuclein at equilibrium with amyloid fibrils [19]. In those cases, the aggregating protein probably had not yet reached true equilibrium; the loss in seeding efficiency of the fibrils, as well as the restricted mobility of the monomer in the gel-like assemblies of fibrils, lead to very long equilibration times. It has been pointed out to us by one of the referees that the combination of fibril growth and higher order assembly of the fibrils and aggregates of fibrils into a gel is akin to combined phase separation and gelation observed in some polymer systems [20]. We will aim in a future study to probe whether the kinetics of these processes can indeed be described by established models of the kind presented in [20].

12 Comparison of *in situ* and *ex situ* ThT aggregation assays

In order to ascertain that the higher order assembly of the α-synuclein fibrils does not simply interfere with their ability to bind Thioflavin-T, we have devised a combined *in situ*/*ex situ* aggregation assay, where one half of an aggregating solution (50 μM monomeric α-synuclein, 2.5 or 0.025 μM seed fibrils) is monitored in real time in a platereader (with 20 μM ThT), whereas the other half is incubated without Thioflavin-T in an incubator at the same temperature (37°C). Aliquots of 25 μl were taken of the solutions incubated without ThT at different times, snap-frozen in liquid nitrogen and stored at -80°C. At the end of the experiment, the aliquots were thawed, 91 μl of water were added, the solution was sonicated for 5s with a sonication probe, and then 4 μl of 500 μM ThT stock solution were added and the fluorescence was immediately measured in a platereader. The rationale behind this experiment is that the higher order aggregates of fibrils that have formed are broken up by the sonication at low ionic strength, such that the ThT can bind to the fibrils. SI Appendix Figure 10 shows the results of this experiment in the case of seed fibrils formed at pH 6.3 that are particularly prone to higher order assembly (see above), in the presence of a significant NaCl concentration of 150 mM. It can be seen that the results from the *in situ* and *ex situ* experiments agree well. We therefore conclude that the higher order assembly/flocculation of the fibrils does not significantly interfere with their ability to bind ThT upon growth, but rather with their overall efficiency of seeding, as shown above.

13 Determination of upper bounds for the *de novo* formation of fibrils through secondary processes

The data at very low seed concentrations (Figure 4 of the main manuscript) can be analysed in detail in order to detect the potential presence of processes that increase the number of growing fibrils. Such processes manifest themselves through positive curvature of the measured fluorescence signal. If we start again with the rate equation for monomer consumption:

$$\frac{dm(t)}{dt} = -\frac{k_+ m_{\frac{1}{2}} P(t) m(t)}{m(t) + m_{\frac{1}{2}}} = -\frac{dM(t)}{dt} \tag{6}$$

where $P(t)$ and $M(t)$ are fibril number and mass concentrations, respectively. The second derivative, and hence the curvature of a plot of fibril mass against time is therefore given by:

$$\frac{d^2M(t)}{dt^2} = -\frac{d^2m(t)}{dt^2} = \frac{k_+ m_{\frac{1}{2}}(m(t)+m_{\frac{1}{2}})(m(t)\frac{dP(t)}{dt} + P(t)\frac{dm(t)}{dt}) - \frac{dm(t)}{dt}(k_+ m_{\frac{1}{2}} P(t) m(t))}{(m(t)+m_{\frac{1}{2}})^2} \tag{7}$$

This expression can be rearranged to obtain a formula for the rate of change of fibril number concentration, $\frac{dP(t)}{dt}$:

$$\frac{dP(t)}{dt} = \frac{\frac{d^2M(t)}{dt^2}(\frac{m(t)}{m_{\frac{1}{2}}}+1)}{k_+ m(t)} - \frac{P(t)\frac{dm(t)}{dt}}{m(t)(\frac{m(t)}{m_{\frac{1}{2}}}+1)} \tag{8}$$

In order to determine absolute upper bounds for this quantity in PBS and in PB, pH 5.2, we computed the numerical second derivatives $\frac{d^2M(t)}{dt^2}$ for the data sets shown in Figure 4 of the main manuscript, and subsequently $\frac{dP(t)}{dt}$, at each point of the data set, assuming that the rate of monomer consumption, $\frac{dm(t)}{dt}$, is dominated by elongation [21]. We do

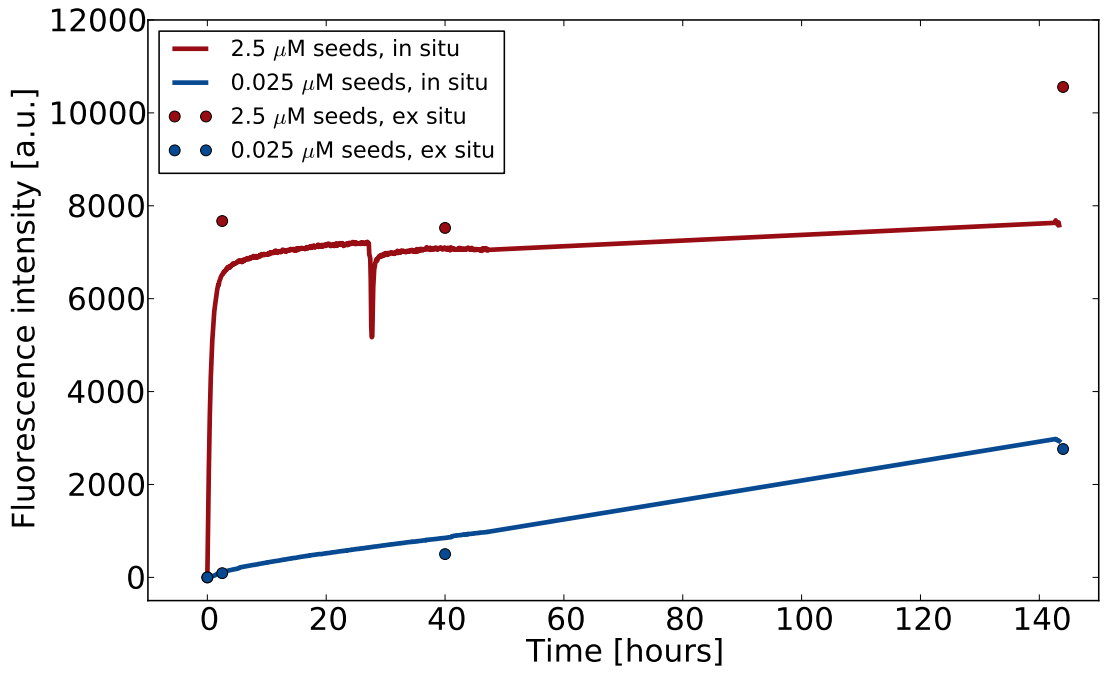

Figure 10: Comparison of *in situ* and *ex situ* ThT aggregation experiment. The experimental procedure is described in detail in the text. The results confirms that the higher order assembly of the fibrils does not significantly interfere with the ThT binding, and therefore *in situ* experiments can be used even under conditions where the higher order assembly is significant (low seed concentrations and high ionic strength).

not have, at present, a model for the secondary nucleation process at low pH, which is required in order to determine the absolute rate constant of secondary nucleation as well as the reaction orders under these different conditions. Therefore, we compare directly the maximal values of $\frac{dP(t)}{dt}$ of the two data sets, which are acquired under comparable conditions of temperature and concentrations of seed fibrils and soluble protein. The maximum of $\frac{dP(t)}{dt}$ in PBS buffer is $1.1{\cdot}10^{-15}\mathrm{Ms}^{-1}$ and in 10 mM phosphate buffer at pH 5.2 $1.6{\cdot}10^{-11}\mathrm{Ms}^{-1}$, four orders of magnitude higher.

14 Analysis of the secondary nucleation process at pH<6

Currently, we do not yet have a mathematical model for the secondary nucleation processes apparent in the aggregation of α-synuclein, preventing us from performing the global fitting strategy presented in [16] and recently employed to describe the aggregation mechanism of the Aβ (1-42) peptide [22]. The currently available models are not suitable, as the higher order assembly of the amyloid fibrils leads to highly spatially inhomogeneous samples, a feature not described by the current aggregation models. In addition, these flocculation processes lead to a decrease in seeding efficiency, which is currently difficult to quantify.
However, the results of our experiments lead us to conclude that the mutiplication of the fibrils is not caused by fragmentation of the growing seed fibrils, but rather by a surface-catalysis process similar to the one recently described for the Aβ (1-42) peptide [22]. Firstly, all of our experiments are performed under quiescent conditions. In particular, in the experiments carried out within microcapillaries, the growing fibrils are not exposed to mechanical stress. In the SI videos of these experiments at low seed concentrations, the time courses of which have been plotted in SI Appendix Figure 11, it is clearly apparent that the higher order assembly/flocculation and subsequent gelation of the fibrils is very pronounced under the conditions where secondary nucleation is observed. It seems unlikely that the growing fibrils within these aggregates are able to fragment easily in the absence of mechanical action.

Further support for the hypothesis that the secondary nucleation is a surface-catalysed process is given by the images shown in Figure 4 e) and f) of the main manuscript. These images show microwells at the end of an aggregation experiment at low seed (3.5 and 35 μM) and low monomomer concentration (10 μM). Interestingly, all the fibrillar protein is localised in small circular aggregates. As expected in this case, at low seed concentration, fewer of these structures can be seen, but they are larger than in the case where 10 times more seeds had been added at the beginning

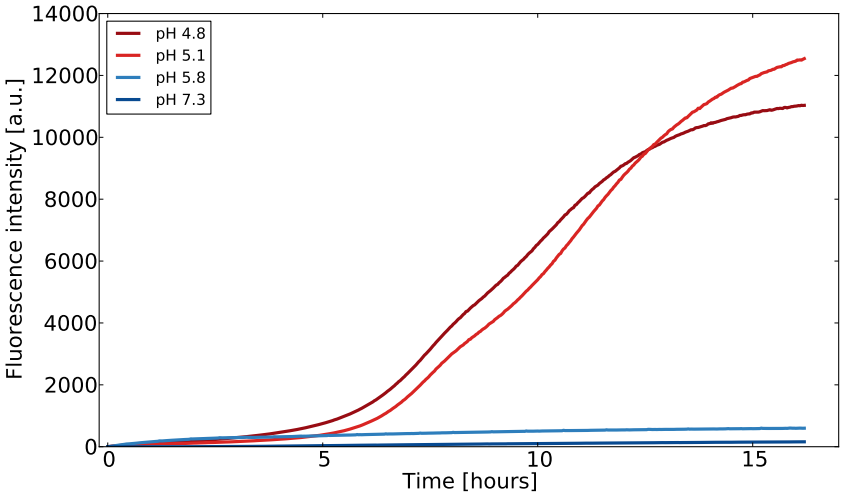

Figure 11: Time courses of fluorescence intensity of aggregation experiments in the presence of low concentrations of seeds in microcapillaries at different pH values (conc. of soluble protein ca. 50 μM, seed concentration < 0.1 %). The corresponding videos can be found as additional SI files (videos S7-S10). As for the bulk experiments, secondary nucleation is clearly apparent at low pH, but not at higher pH. In the videos, the flocculation and gelation of the fibrils at low pH is also very clearly apparent. We explicitly note here that the experiments in microcapillaries, both at high and low seed concentrations, clearly demonstrate that an air-water interface is not needed for fibril elongation and secondary nucleation, contrary to what has been reported in a recent study [23].

of these experiments (see histograms in the insets of the Figure).
It therefore appears that under these pH conditions, close to the isoelectric point of α-synuclein, the seed fibrils immediately form small microscopic aggregates, which then grow and spread, but the newly formed aggregates are not able to detach from the origin of their nucleation. This picture of the process is very consistent with the generally accepted knowledge about the aggregation of α-synuclein, discussed in detail in the main manuscript, namely that the primary nucleation is surface- (or surfactant-) catalysed in all cases.
The picture that therefore emerges for the aggregation of α-synuclein is that, depending of the solution pH and the ionic strength, the amyloid fibrils are highly prone to form higher order aggregates, a process that decreases the accessibility of the growing ends and therefore the seeding efficiency. At low pH values close to the isoelectric point, this phenomenon is very pronounced, however, at the same time the aggregates of fibrils apepar to have surface properties amenable to secondary nucleation. Therefore the balance between growth and (secondary) nucleation processes is very strongly dependent on the solution conditions.

15 The charge of α-synuclein as a function of pH

The sharp pH-dependence of the secondary process is most likely related to the titration of carboxylate groups in the acidic C-terminus of monomer and fibril. SI Appendix Figure 12 shows the net charge of the protein calculated as a function of pH based on the pK_a values and Hill coefficients reported for 250 μM α-syn in 20 mM PB [24]. While the single histidine (H50) has a pK_a value at 6.8, the ca 4.4 units calculated change in net charge between pH 6 and 5 is mainly due to partial protonation of several carboxylate groups in the protein, especially in the acidic C-terminus which containing 16 carboxylates, 13 of which have elevated pK_a values [24]. At lower protein concentration and buffer strength, as in the present study, as well as in the fibril with many negative groups close together, these pK_a values will most likely be even more up-shifted in line with the salt dependence of α-synuclein pK_a values [24] and previous studies [25, 26].

References

[1] Hoyer, W, Antony, T, Cherny, D, Heim, G, Jovin, T. M, & Subramaniam, V. (2002) Dependence of alpha-synuclein aggregate morphology on solution conditions. *J Mol Biol* **322**, 383–393.

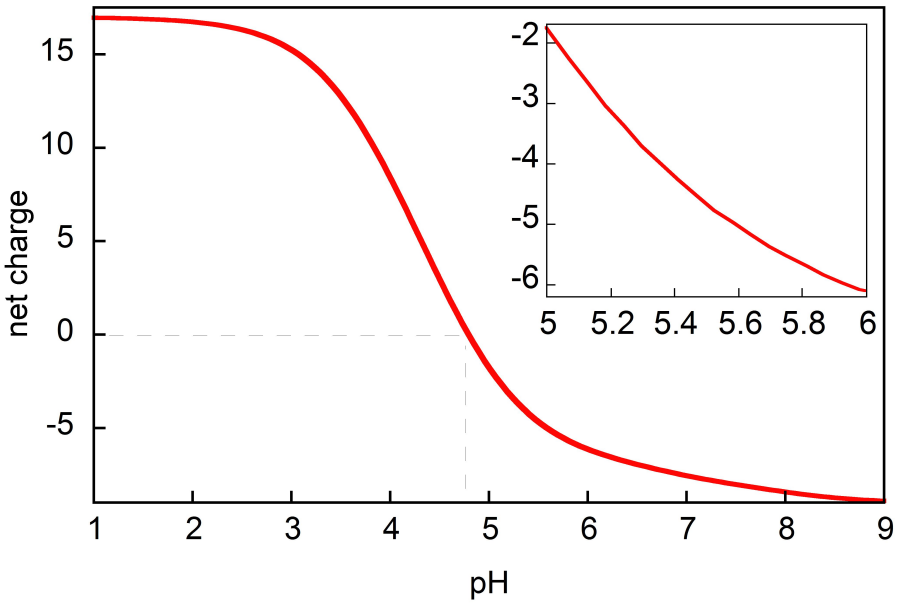

Figure 12: Net charge of α-synuclein calculated as a function of pH based on the pKa values and Hill coefficients reported for 250 μM -syn in 20 mM NaP [24]. The inset shows the calculated net charge between pH 5 and 6. For each aspartate, glutamate or C-terminus the charge is calculated as charge = -1/(1 + $10^{pK_a - pH}$) and for the histidine and N-terminus, charge = 1 - 1/(1 + $10^{pK_a - pH}$). The N-terminal pK_a value was not reported in [24], so we assume a model value of 8.0. For lysines and arginines a constant charge of +1 was assumed between pH 0 and 9.

[2] Buell, A. K, Blundell, J. R, Dobson, C. M, Welland, M. E, Terentjev, E. M, & Knowles, T. P. J. (2010) Frequency factors in a landscape model of filamentous protein aggregation. *Phys Rev Lett* **104**, 228101.

[3] Bartels, T, Choi, J. G, & Selkoe, D. J. (2011) -synuclein occurs physiologically as a helically folded tetramer that resists aggregation. *Nature*.

[4] Eliezer, D, Kutluay, E, Bussell, R, & Browne, G. (2001) Conformational properties of alpha-synuclein in its free and lipid-associated states. *J Mol Biol* **307**, 1061–1073.

[5] Waudby, C. A, Camilloni, C, Fitzpatrick, A. W. P, Cabrita, L. D, Dobson, C. M, Vendruscolo, M, & Christodoulou, J. (2013) In-cell nmr characterization of the secondary structure populations of a disordered conformation of -synuclein within e. coli cells. *PLoS One* **8**, e72286.

[6] Burr, J, Vivona, S, Diao, J, Sharma, M, Brunger, A. T, & Sdhof, T. C. (2013) Properties of native brain -synuclein. *Nature* **498**, E4–6; discussion E6–7.

[7] Bousset, L, Pieri, L, Ruiz-Arlandis, G, Gath, J, Jensen, P. H, Habenstein, B, Madiona, K, Olieric, V, Bckmann, A, Meier, B. H, & Melki, R. (2013) Structural and functional characterization of two alpha-synuclein strains. *Nat Commun* **4**, 2575.

[8] Khurana, R, Coleman, C, Ionescu-Zanetti, C, Carter, S. A, Krishna, V, Grover, R. K, Roy, R, & Singh, S. (2005) Mechanism of thioflavin T binding to amyloid fibrils. *J Struct Biol* **151**, 229–238.

[9] Grey, M, Linse, S, Nilsson, H, Brundin, P, & Sparr, E. (2011) Membrane interaction of α-synuclein in different aggregation states. *J Parkinsons Dis* **1**, 359–371.

[10] Buell, A. K, Dhulesia, A, White, D. A, Knowles, T. P. J, Dobson, C. M, & Welland, M. E. (2012) Detailed analysis of the energy barriers for amyloid fibril growth. *Angew Chem Int Ed Engl* **51**, 5247–5251.

[11] Uversky, V. N, Li, J, & Fink, A. L. (2001) Evidence for a partially folded intermediate in alpha-synuclein fibril formation. *J Biol Chem* **276**, 10737–10744.

[12] Morris, A. M & Finke, R. G. (2009) Alpha-synuclein aggregation variable temperature and variable ph kinetic data: a re-analysis using the finke-watzky 2-step model of nucleation and autocatalytic growth. *Biophys Chem* **140**, 9–15.

[13] Buell, A. K, Hung, P, Salvatella, X, Welland, M. E, Dobson, C. M, & Knowles, T. P. J. (2013) Electrostatic effects in filamentous protein aggregation. *Biophys J* **104**, 1116–1126.

[14] Manno, M, Mauro, M, Craparo, E. F, Podest, A, Bulone, D, Carrotta, R, Martorana, V, Tiana, G, & Biagio, P. L. S. (2007) Kinetics of different processes in human insulin amyloid formation. *J Mol Biol* **366**, 258–274.

[15] Knowles, T. P. J, Shu, W, Devlin, G. L, Meehan, S, Auer, S, Dobson, C. M, & Welland, M. E. (2007) Kinetics and thermodynamics of amyloid formation from direct measurements of fluctuations in fibril mass. *Proc Natl Acad Sci U S A* **104**, 10016–10021.

[16] Knowles, T. P. J, Waudby, C. A, Devlin, G. L, Cohen, S. I. A, Aguzzi, A, Vendruscolo, M, Terentjev, E. M, Welland, M. E, & Dobson, C. M. (2009) An analytical solution to the kinetics of breakable filament assembly. *Science* **326**, 1533–1537.

[17] Smith, J. F, Knowles, T. P. J, Dobson, C. M, Macphee, C. E, & Welland, M. E. (2006) Characterization of the nanoscale properties of individual amyloid fibrils. *Proc Natl Acad Sci U S A* **103**, 15806–15811.

[18] Israelachvili, J. (1992) *Intermolecular and surface forces.* (Academic Press).

[19] Wood, S. J, Wypych, J, Steavenson, S, Louis, J. C, Citron, M, & Biere, A. L. (1999) alpha-synuclein fibrillogenesis is nucleation-dependent. implications for the pathogenesis of parkinson's disease. *J Biol Chem* **274**, 19509–19512.

[20] Sciortino, F, Bansil, R, Stanley, H. E, & Alström, P. (1993) Interference of phase separation and gelation: A zeroth order kinetic model. *Phys Rev E* **47**, 4615–4618.

[21] Cohen, S. I. A, Vendruscolo, M, Welland, M. E, Dobson, C. M, Terentjev, E. M, & Knowles, T. P. J. (2011) Nucleated polymerization with secondary pathways. I. time evolution of the principal moments. *J Chem Phys* **135**, 065105.

[22] Cohen, S. I. A, Linse, S, Luheshi, L. M, Hellstrand, E, White, D. A, Rajah, L, Otzen, D. E, Vendruscolo, M, Dobson, C. M, & Knowles, T. P. J. (2013) Proliferation of amyloid-42 aggregates occurs through a secondary nucleation mechanism. *Proc Natl Acad Sci U S A* **110**, 9758–9763.

[23] Campioni, S, Carret, G, Jordens, S, Nicoud, L, Mezzenga, R, & Riek, R. (2014) The presence of an air-water interface affects formation and elongation of alpha-synuclein fibrils. *J Am Chem Soc.*

[24] Croke, R. L, Patil, S. M, Quevreaux, J, Kendall, D. A, & Alexandrescu, A. T. (2011) NMR determination of pKa values in α-synuclein. *Protein Sci* **20**, 256–269.

[25] Kesvatera, T, Jönsson, B, Thulin, E, & Linse, S. (1996) Measurement and modelling of sequence-specific pKa values of lysine residues in calbindin D9k. *J Mol Biol* **259**, 828–839.

[26] Lindman, S, Linse, S, Mulder, F. A. A, & Andr, I. (2006) Electrostatic contributions to residue-specific protonation equilibria and proton binding capacitance for a small protein. *Biochemistry* **45**, 13993–14002.

Supporting Information

Buell et al. 10.1073/pnas.1315346111

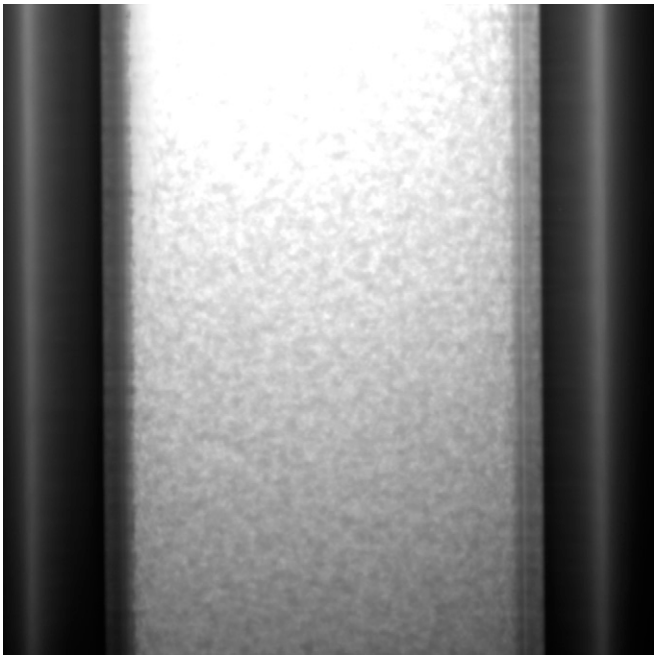

Movie S1. Seeded aggregation in a glass microcapillary; ~100 μM α-synuclein, 20 mM phosphate buffer (PB), pH 6.3, ~10 μM ThT, ~2.5 μM seeds (formed at pH 6.3).

Movie S1

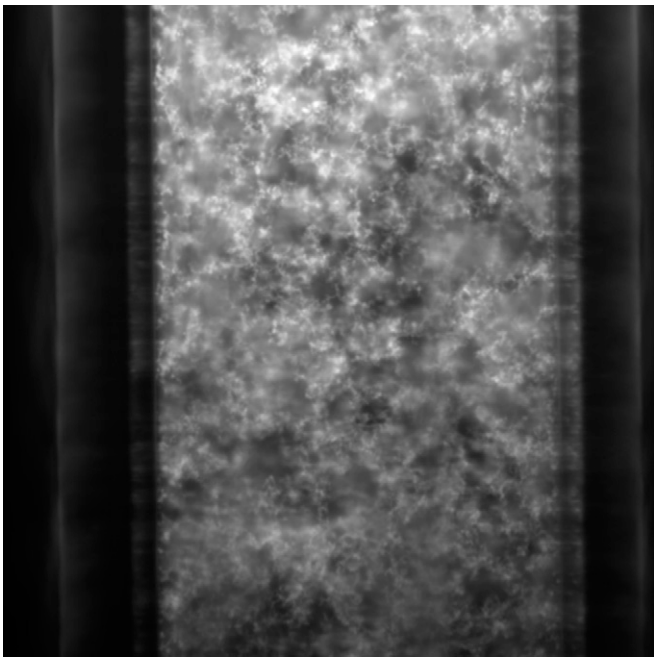

Movie S2. Seeded aggregation in a glass microcapillary; ~100 μM α-synuclein, 20 mM PB, pH 6.3, 150 mM NaCl, ~10 μM ThT, ~2.5 μM seeds (formed at pH 6.3).

Movie S2

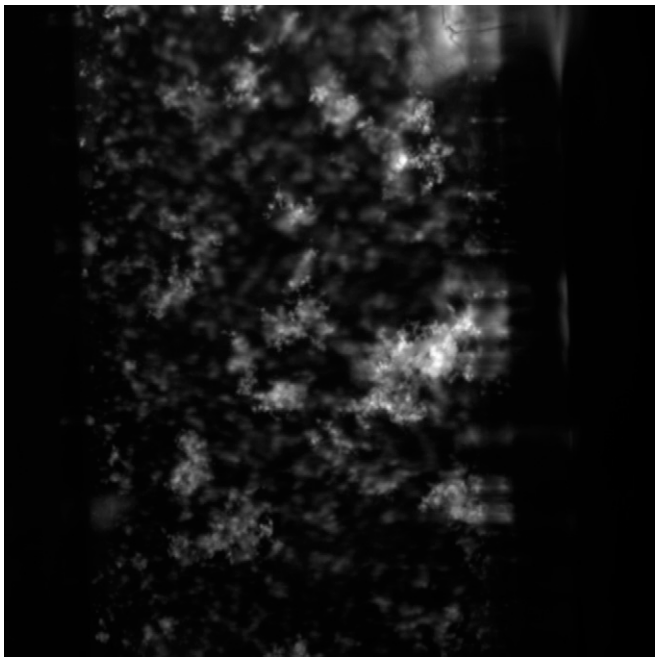

Movie S3. Seeded aggregation in a glass microcapillary; ~100 μM α-synuclein, 20 mM PB, pH 6.3, 50 mM $CaCl_2$, ~10 μM ThT, ~2.5 μM seeds (formed at pH 6.3).

Movie S3

Movie S4. Seeded aggregation in a glass microcapillary; ~100 μM α-synuclein, 10 mM PB, pH 6.3, ~10 μM ThT, ~2.5 μM seeds (formed at pH 6.3).

Movie S4

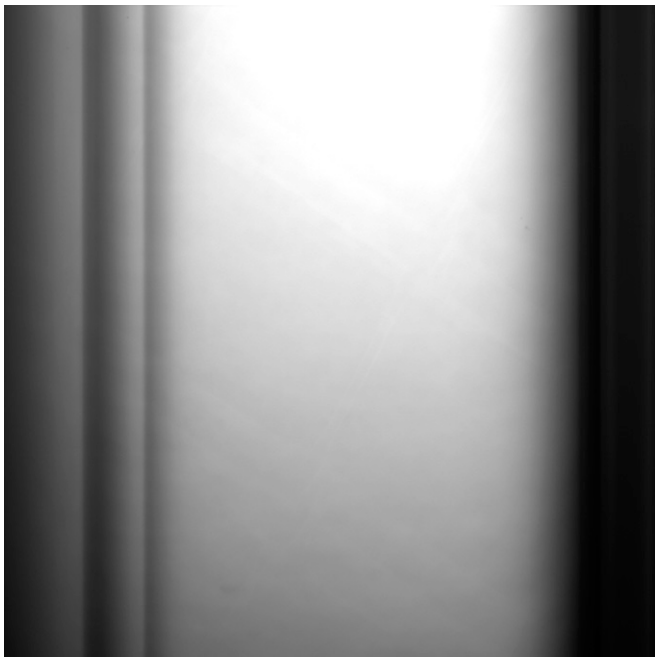

Movie S5. Seeded aggregation in a glass microcapillary; ~100 μM α-synuclein, 20 mM PB, pH 6.3, ~10 μM ThT, ~2.5 μM seeds (formed at pH 7.4).

Movie S5

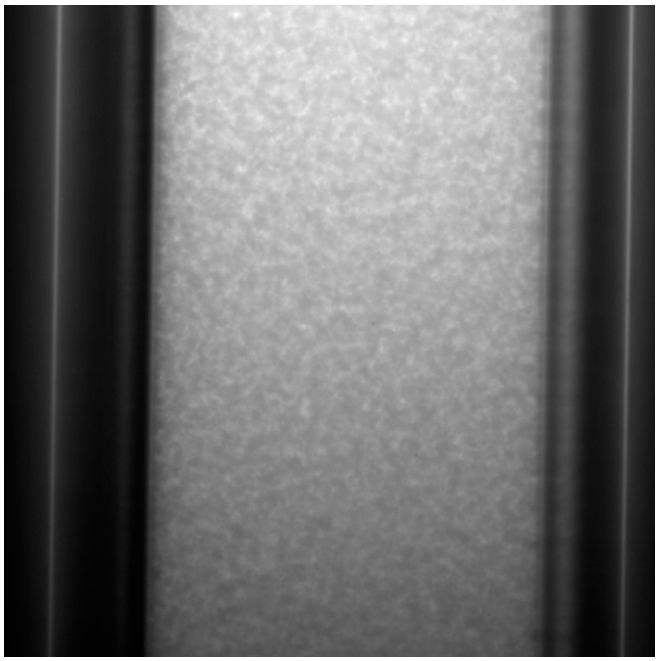

Movie S6. Seeded aggregation in a glass microcapillary; ~100 μM α-synuclein, 20 mM PB, pH 7.4, ~10 μM ThT, ~2.5 μM seeds (formed at pH 7.4).

Movie S6

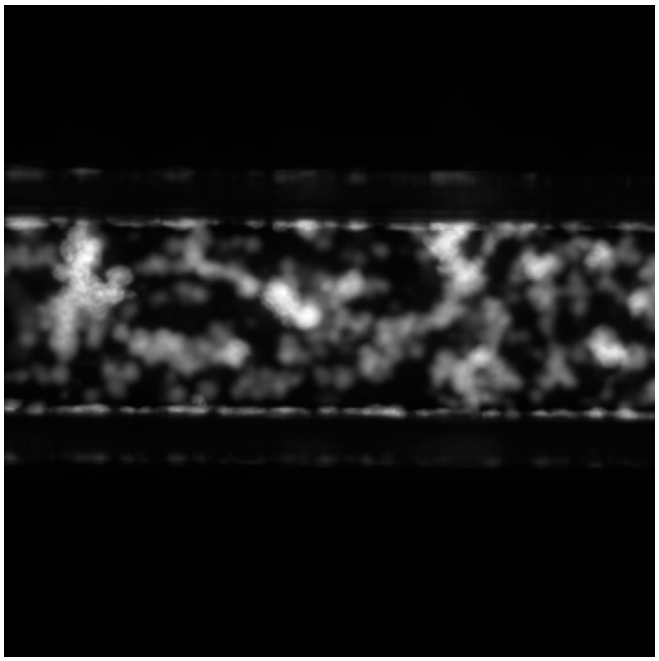

Movie S7. Seeded aggregation in a glass microcapillary; ~50 μM α-synuclein, 10 mM PB, pH 4.8, ~30 μM ThT, ~20 nM seeds (formed at pH 6.3).

Movie S7

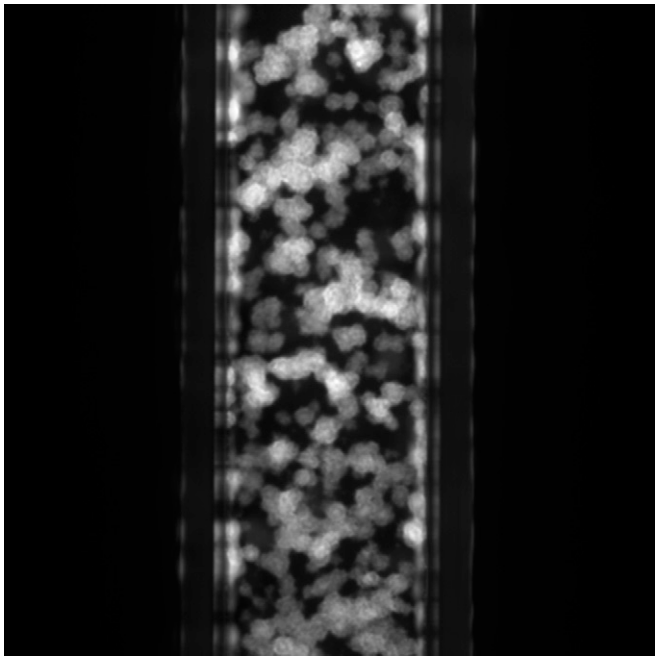

Movie S8. Seeded aggregation in a glass microcapillary; ~75 μM α-synuclein, 10 mM PB, pH 5.1, ~30 μM ThT, ~20 nM seeds (formed at pH 6.3).

Movie S8

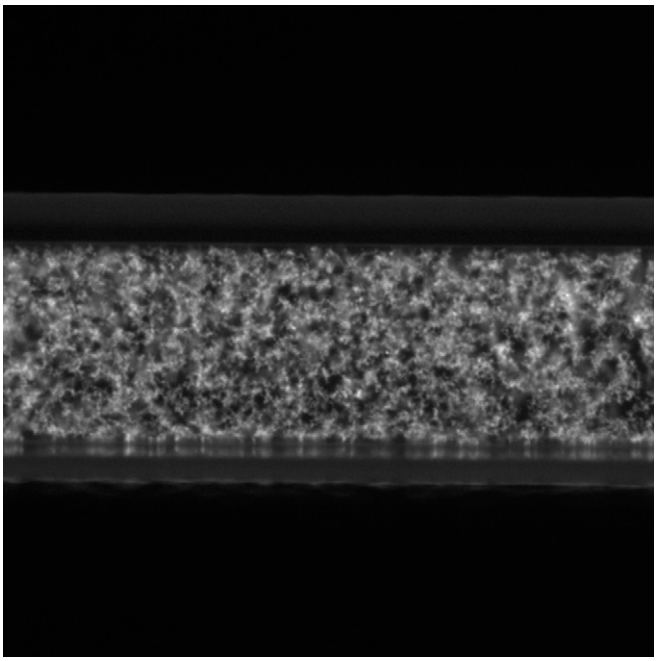

Movie S9. Seeded aggregation in a glass microcapillary; ~50 μM α-synuclein, 10 mM PB, pH 5.8, ~35 μM ThT, ~50 nM seeds (formed at pH 6.3).

Movie S9

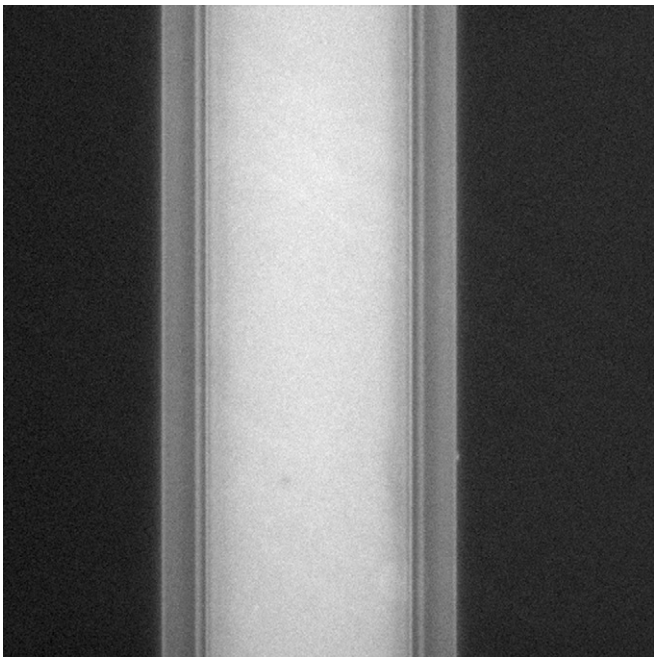

Movie S10. Seeded aggregation in a glass microcapillary; ~50 μM α-synuclein, 10 mM PB, pH 7.3, ~20 μM ThT, ~50 nM seeds (formed at pH 6.3).

Movie S10

Other Supporting Information Files

SI Appendix (PDF)